

A STUDY OF THE CHARACTERISTICS AND LIMITATIONS OF VARIOUS PLATINGS  
ON CYLINDRICAL ELECTRICAL CONDUCTORS

by

ROBERT C. SCULLY

Presented to the Faculty of the Graduate School of  
The University of Texas at Arlington in Partial Fulfillment  
of the Requirements  
for the Degree of

DOCTOR OF PHILOSOPHY

THE UNIVERSITY OF TEXAS AT ARLINGTON

December 2013

Copyright © by Robert C. Scully 2013

All Rights Reserved

## Acknowledgements

This work might never have been completed without the patience and understanding of Dr. Jonathan Bredow, my advisor for it seems too many years to number. His constancy and quiet demeanor gave me the strength and resolve to see this through in spite of life's adversities and setbacks. I also would like to acknowledge the support of my co-workers and my professional colleagues, without who I would have given up long ago. Last, and certainly not least, I want to mention the love and support from my wife and lifelong companion, Elizabeth, a guiding star through thick and thin, and most importantly in the darkest days of my despair, as I struggled through this process.

November 20, 2013

## Abstract

# A STUDY OF THE CHARACTERISTICS AND LIMITATIONS OF VARIOUS PLATINGS ON CYLINDRICAL ELECTRICAL CONDUCTORS

Robert C. Scully, PhD

The University of Texas at Arlington, 2013

Supervising Professor: Jonathan Bredow

This work explores the impedance characteristics of copper wires plated with tin, silver, or nickel, the most common type of wiring used in the computer, communications, and aerospace industries. The background of plated wires and a brief review of related research is provided. This is followed by a detailed development of the theory of plated wires, accompanied by a MAPLE code in the appendix that can be used for the numerical analysis of plated wires having two or more plating layers. The code was used to generate a series of curves predicting the impedance behavior of both solid, "pure" metals, as well as copper wire plated with silver, tin, and nickel. Additional curves are provided highlighting the very interesting impedance behavior of nickel plated copper wire. All of these curves are accompanied by a number of observations to point out the more interesting aspects of the behavior. Several impedance measurements of commonly available military specification plated wire stranded conductors are then discussed. A number of the attempted measurements were unable to resolve the very small impedances. Even so, a last attempt worked very well to demonstrate the predicted impedance behavior, as evidenced by the measured raw data curves shown in contrast to the same curves with fixture parasitics removed. Insertion loss measurements were then made of commonly available military specification plated wire twisted shielded pair

that provided further confirming evidence for the predictions made from the numerical analysis. In all cases, observations and comments are provided to explain why some measurements were superior to others, and why certain steps were taken to defeat interference from clouding the results. The document closes with recommendations for future efforts and concluding remarks.

## Table of Contents

Acknowledgements .....	iii
Abstract.....	iv
List of Illustrations .....	viii
Chapter 1 Introduction.....	1
1.1 Understanding the root of the problem .....	1
1.2 A bit of history .....	3
1.3 A general discussion of the plating of copper wire .....	3
1.4 Tin plating of copper wire.....	5
1.5 Silver plating of copper wire.....	6
1.6 Nickel plating of copper wire .....	6
1.7 Closing comments .....	8
Chapter 2 Review of some related early and contemporary research.....	10
2.1 Skin effect.....	10
2.2 Layered or coated conductors .....	12
Chapter 3 Foundational Theory.....	17
3.1 Solid homogeneous cylindrical conductors .....	17
3.1.1. Current density .....	17
3.1.2. Impedance.....	21
3.2 Solid cylindrical conductors with plating layers .....	22
3.2.1. Current density .....	22
3.2.2. Impedance.....	28
Chapter 4 Measurements.....	37
Chapter 5 Discussion .....	53
Chapter 6 Highlights and Concluding Remarks.....	62

Appendix A MAPLE Code for Numerical Computation of the Impedance of Plated Wire.....	64
References.....	70
Biographical Information .....	76

## List of Illustrations

Figure 2-1 Cross section of Cu core with Ni layer [39] .....	15
Figure 3-1 Cross section of cylindrical conductor.....	17
Figure 3-2 Cross section of a cylindrical conductor with a single plating layer .....	23
Figure 3-3 Impedance behavior of pure metals.....	29
Figure 3-4 Impedance behavior of coated metals .....	30
Figure 3-5 Ni relative permeability as a function of frequency.....	31
Figure 3-6 Comparison: “Pure” Ni vs “pure” Cu vs Cu plated with 50 $\mu\text{m}$ of Ni .....	34
Figure 3-7 Comparison: “Pure” Ni vs “pure” Cu vs Cu plated with 161 $\mu\text{m}$ of Ni .....	35
Figure 3-8 Comparison: “Pure” Ni vs “pure” Cu vs Cu plated with 2330 $\mu\text{m}$ of Ni .....	36
Figure 4-1 1 <sup>st</sup> measurement attempt setup [63] .....	39
Figure 4-2 2 <sup>nd</sup> measurement attempt fixture [64].....	40
Figure 4-3 TRL standards on design sketches.....	42
Figure 4-4 Thru TRL standard.....	43
Figure 4-5 Open TRL standard .....	43
Figure 4-6 Line TRL standard .....	44
Figure 4-7 Improved Wetterlin fixture .....	45
Figure 4-8 Data captured using the improved Wetterlin fixture .....	46
Figure 4-9 Corrected data using the improved Wetterlin fixture .....	47
Figure 4-10 General insertion loss setup .....	49
Figure 4-11 Close-up of wire connected to baluns.....	49
Figure 4-12 Close-up of balun nomenclature plate .....	50
Figure 4-13 Suppression of common mode noise in VNA measurement [74].....	51
Figure 4-14 S21 data for twisted shielded wire pairs.....	52
Figure 5-1 Figure 6 from Fowler [38].....	55



Figure 5-2 Figure 7 from Fowler [38].....	56
Figure 5-3 Figure by Graf [39].....	56
Figure 5-4 SCSI PIP Committee presentation [75].....	57

## Chapter 1

### Introduction

Electrical and electronic hardware designed and built for use in the computer, communications, and aerospace industries must incorporate protection from high speed transients and radio frequency interference that can enter the equipment via its interconnecting wiring harness. To this end, equipment has traditionally been designed with input/output filtering, either included in the circuitry or embedded in connectors leading external to the equipment. Often times, such design is not incorporated until late in the design process, after the equipment has failed either its power quality or electromagnetic interference control certification testing, or both! This can be a significant cost, mass, and volume driver for equipment design, and can introduce serious delay into the production and release of equipment onto the open market. Using a distributed means of providing such filtering in interconnecting wiring harness external to the equipment would immediately impact these design drivers in a positive fashion, facilitating smaller, more efficient, less costly designs.

#### 1.1 Understanding the root of the problem

Wire used for equipment interconnections is typically not well understood by many practicing electrical or electronics engineers, who more often than not consider it simply as a convenient means of transferring electrical signals from one point to another within a circuit, exhibiting minimal impedance and near infinite bandwidth. Indeed, the “characteristics of wire” as a topic is not generally taught as part of a standard university level electrical engineering curriculum. Students learn about topics such as a single wire above an infinite ground plane, infinite two wire transmission lines with conductor separation large enough to dispense with any concerns over proximity effects or altered dielectric constants, and basic coaxial cable design. But very few, if any, courses deal

with the subtleties and design constraints associated with twisted non-shielded or shielded pair wiring that is ubiquitous across industry. Radio Frequency (RF) engineers working with higher frequencies for wireless networks, and printed circuit board designers faced with increasingly faster clock and circuit switching speeds, are now being more exposed to advanced transmission line theory, but these engineers are more often dealing with microwave link coverage and margin concerns or circuitry design issues, as opposed to interconnecting wires that join everything together at the subsystem and system levels. Computer equipment and network engineers are faced with steadily increasing speeds over copper interconnects, and the industry is rife with misunderstanding regarding how the interconnecting wire works, or how it could be designed to improve crosstalk or data rate performance.

In contrast, power system and ElectroMagnetic Compatibility (EMC) engineers routinely consider system voltage drops over long wire runs for operational safety considerations and often engage in discussions and calculations wherein the distributed parameters of resistance, inductance and capacitance of such wire runs are a necessary part of a design. As an example, line impedance simulation networks (LISNs) that incorporate estimated series inductance, resistance, and parallel capacitance are often used in standard power quality and electromagnetic interference testing to introduce “real world” electrical line characteristic effects into equipment set-ups for demonstration of compliance to various conducted and radiated emissions and susceptibility criteria. Calculations such as are described here are seldom performed by other electrical or electronic engineers, who in general are not thinking about the distributed effects of wire on their sub-systems. These same engineers are also often not thinking about input and output filters to control undesirable noise from entering or exiting their hardware, or transient protection devices to control current and voltage impulses arising from load

switching or external influences such as lightning and electrostatic discharge. When they do think about filters and transient protection, their designs tend to grow in volume and mass, and of course in cost. Additional components introduce vibration and mechanical shock concerns, and reduce reliability.

## 1.2 A bit of history

Metal formed into wire has been used since biblical times, according to references contained in the Bible, Exodus XXXIX. Originally, wire was most likely formed by beating out flat, narrow strips of metal, and then shaping them into a cylindrical shape, perhaps by filing the edges. In some cases, flat strips of noble metals might be cut into very fine wires, or threads, used for weaving. The process of forming wire by drawing metal through successively smaller circular holes in a hardened metal plate, as is utilized today, is believed to have originated in the fourteenth century with Rudolph of Nurnberg. In 1570, Anthony Fournier introduced a number of refinements to the art of forming wire through the drawing process, and was able to produce exceedingly thin wire. In 1592, Frederick Hegelsheimer of Nurnberg was granted a patent from the Nurnberg magistrates for the production of copper wire coated with gold or silver [1]. Sheffield Plated wire, made in England, was originally formed by the cohesion of thin sheets of silver to previously drawn copper wire using an application of heat and burnishing tools. In 1768, a plater in Birmingham named George Whateley filed two patents for making plated drawn wire. Whateley's patents addressed silver plating over copper wire, gold plating over silver wire, and gold plating over silver plated copper [2].

## 1.3 A general discussion of the plating of copper wire

Bare, virgin copper is relatively free of corrosion effects, tending to form a combined thin layer of copper oxides and copper sulfides that act to retard further corrosion. Unfortunately, these oxides and sulfides exhibit low conductivity, and if allowed

to penetrate into interconnections, or wick into stranded conductors, can measurably impact electrical and thermal performance. The formation of copper oxides and sulfides is accelerated by temperature and can occur as part of the aging process of wire insulation as the materials outgas over time. Sulfidation of bare copper wire insulated with vulcanized rubber was a major problem for older house wiring installations, and prompted the use of tin plating as a means of control. Exposure to a salt water environment can exacerbate galvanic corrosion between bare copper and a variety of other materials, such as nickel, steel, and aluminum, all common engineering materials found in electrical, electronic, and aerospace applications. Modern copper wire used for these applications is plated for many other reasons, including the enhancement of solderability, and to prevent accelerated oxidation of the copper during high-temperature service, thereby extending the operating temperature range. Plating with silver acts to enhance the electrical performance of wiring used for circuits operating at frequencies of a few hundred kilohertz and above, and extends the operating temperature range up to 200 degrees centigrade. Plating provides a barrier between the copper core and insulation materials, such as rubber, that would react with the copper and adhere to it, or promote corrosion via the aging process.

But plating the wire introduces new complexity with respect to electromagnetic performance. Cylindrical copper conductors, routinely plated with tin, silver, or nickel, are found throughout the electrical, electronic, and aerospace industries. While each of these plating metals offers unique advantages over bare copper wire, they all interact with copper in a metallurgic sense as well as an electromagnetic sense, resulting in intermetallic growth, metal migration, and potential galvanic corrosion issues.

The plating of copper wire used for electrical and electronic purposes using pure tin, tin-lead alloys, silver, or nickel, is accomplished today with precision, in adherence to

various specifications [3-9]. Copper wire can be plated by hot dipping in a molten metal bath, electroplating, or cladding. With the advent of continuous processes, electroplating has become the dominant process, especially because it can be completed easily and in sequence, either prior to or following the wiredrawing operation. These processes can be controlled to produce relatively uniform plating thicknesses ranging from 1 micron to more than 50 microns, depending on the application.

#### 1.4 Tin plating of copper wire

Copper wire plated with pure tin, or a tin alloy, is the type of plated wire most commonly found throughout the electrical, electronic, and aerospace industries. Tin plating provides sacrificial protection for copper and arrests corrosion caused by sulfur bearing reagents. It enhances solderability in newly produced wire and increases the operating temperature range for copper up to 150° C. A long term drawback for tin plated wire is the formation of copper tin intermetallics at the interface between the two metals. Given sufficient time, the intermetallic formation process will completely convert the layer of tin plating to a solid layer of copper tin intermetallic, resulting in a surface that is very difficult to solder and that cannot be easily cleaned without mechanical removal of the surface of the wire. Another serious drawback is that tin plated wire cannot be used with common insulation materials that require high-temperature processing, such as polytetrafluoroethylene (PTFE; also known as Teflon), fluorinated ethylene propylene (FEP), ethylene-tetrafluoroethylene (ETFE; also known as Tefzel), and polyimide film, more commonly known by the DuPont brand name Kapton. Note that all of these materials are commonly used as wire jacketing material by the military and commercial aerospace industries. Non-aerospace industry, particularly in computer networking applications, still relies on lower temperature, and less expensive, jacketing materials such as polyvinyl chloride (PVC).

### 1.5 Silver plating of copper wire

Silver plated copper wire may exhibit exceptional electrical conductivity at higher frequencies and may be particularly useful in RF applications where skin effect plays a significant role, possibly allowing the use of smaller diameter conductors. It offers good immunity to corrosion under exposure to high processing and operating temperatures up to 200°C. Unlike tin plated wire, no intermetallics form between the plating and the underlying copper, and so silver plated wire has excellent solderability, whether new off the shelf or after many years of exposure to uncontrolled environments. One significant drawback is that the silver surface may react with substances such as glycol to produce a potential flammability hazard. Another is that silver plated wire has a slightly higher cost than other platings. Larger gauge wires, such as AWG 0, cannot be used with this finish as cold welding at points of contact between the wire strands may increase wire rigidity. Finally, silver plated wire is subject to a corrosion process known as red plague [10]. Red plague is the formation of cuprous-oxide, possibly together with some black cupric oxide, coincident with the presence of a silver-copper galvanic cell existing at poorly plated locations or locations that exhibit a compromised or damaged plating surface. The corrosion process is driven by oxygen in the presence of moisture acting as an electrolyte. If not stopped, the corrosion process will continue until all the copper is destroyed, leaving only a shell formed of the silver plating and a core of copper oxide.

### 1.6 Nickel plating of copper wire

Nickel plated wire is more expensive than tin plated wire, and is less expensive than silver plated wire. It offers superior corrosion control and strength when compared to either tin or silver plating. It extends the useful operating temperature range of plated copper wire up to 260°C while still exhibiting good flexibility after long-term aging at 200°C. An excellent discussion of the merits of nickel plating on conductors was published

by Sarkuysan Electrolytic Copper Company [11]. A big drawback is that nickel plated wire is very difficult to solder with non-activated fluxes. Even with the use of activated fluxes, it has a variable solderability, dependent on the type and thickness of the nickel plating. Moreover, the flux may wick under the insulation and promote corrosion long after the soldering process is complete. Otherwise, nickel plated wire is not susceptible to corrosion over a wide range of applications. Crimpability is fairly good, but ohmic resistance varies with cleanliness of the surface, paramount to long term success and reliability. Depending on the plating layer thickness, nickel-plated conductors may exhibit anywhere from 4% to 30% higher resistivity than virgin copper wire, with a correspondingly higher insertion loss in a given circuit application. Nickel plated wire may exhibit a magnetic moment that can be detected by an external observer or that can introduce unsuitable perturbations into magnetically sensitive spacecraft experiments. A very interesting application of nickel plated copper wire that capitalized on the magnetic properties of nickel plating was developed and refined to a high degree of success during the late 1950s and throughout the 1960s [12-16]. Moderate lengths of copper wire plated with a nickel-iron ferrite material were arrayed in a mechanical matrix. These arrays were referred to as plated wire memory cells. Arrays of this ilk were used successfully in a plethora of high-speed memory applications, including the Remington Rand UNIVAC 1110 computer, all UNIVAC 9000 series computers, the Minuteman III missile, the Viking Mars Lander, the LANDSAT-D satellite, and the Hubble Space telescope.

Related to nickel plating of copper wire is the use of ferrite sheathing in the insulation of copper wire to produce a distributed filtering action. In so-called FilterLine wire [17], controlled by specifications MIL-C-85485 and SAE AS85485, the electrical energy associated with high-speed transients and high-frequency noise components above 100 MHz is trapped in the ferrite layer by an overlying metallic shield, and is



therein dissipated. Similar commercial applications, one made by EMC Eupen [18,19], one made by Intermark [20], and one made by ARC Technologies [21], also incorporate ferrite material into the wire sheathing, but do not rely on the presence of a metallic shield for the associated attenuation.

### 1.7 Closing comments

All of the foregoing serves to underscore the impact of plating on common copper wire and alludes to the complexity of the topic, as well as the potential versatility of the use of plated wire as more than just a convenient means of transferring electrical signals from one point to another within a subsystem or system.

The need for filtering and transient protection is of course real, and is dictated by the needs of the particular design, but nonetheless can be restrictive in many applications. The distributed nature of wire characteristics is also real, and that physics comes along with the use of wire, whether it is desired or not. But instead of considering the characteristics of the wire as additional system complexity, why not intentionally utilize the wire to aid in the filtering and transient protection that will be a necessary part of the circuitry anyway? Doing so can alleviate some of the volume, mass, and cost impact of additional components, while capitalizing on the presence of the wires that have to be used to interconnect everything. Wire itself, in useful configurations such as power distribution lines and twisted shielded pairs for signal lines, has demonstrable impedance characteristics that are a function of frequency. Plated wire has demonstrated characteristics that are also functions of frequency, independent of harness configuration. Careful design that intentionally integrates the fundamental characteristics of wire configurations with those associated with the presence of plating materials offers the possibility of interference control and attenuation as a function of frequency that can

expand the functionality of the wiring harness and offset the burden of filtering and transient protection, precisely what is often needed in the terminal equipment.

One basis for such a design approach lies in clearly understanding the electromagnetic characteristics of plated wire and how they might be manipulated to best advantage. This work will explore this understanding, and point the way forward to future research to more fully develop this design approach. In Chapter 2, a brief survey is provided of historical and contemporary work that touches on the underlying physics and that has impacted this work in a direct sense. In Chapter 3, the basic electromagnetic theory for current density and impedance of cylindrical conductors is discussed and developed for a homogeneous metallic wire. The theory is then modified to account for the presence of one or more plating layers of varying material types and thicknesses. Chapter 4 describes some of the attempts at measurement of the impedance of a short length of plated wire, and the difficulties encountered in this approach, including a successful attempt and the necessary extraction of parasitics to clearly show the measured data. This is followed by a description of insertion loss measurements of sample plated wire twisted shielded pairs, the results of which combined with the theoretical development and results reported in previously cited works in Chapter 2 and the successful measurements of the single conductor configuration illustrate the efficacy of using nickel plating as a means of intentionally introducing attenuation as a function of applied frequency. Highlights of the results are examined in Chapter 5, focusing on the observations gleaned during the analysis and measurement processes. Concluding discussions center on the natural further development of this research, including planned future work and collaborative efforts.

## Chapter 2

### Review of some related early and contemporary research

The study of plated wires involves a complex number of different engineering aspects, including metallurgy, materials science, and of course electromagnetics. The subject is accordingly broad in nature. The research in this work focuses on the electromagnetics of the topic, and this chapter provides a brief survey of some of the historical and more contemporary efforts that touch the root of that physics, and that in some way influenced this work.

### 2.1 Skin effect

Maxwell wrote [22] “When the current in a wire is of varying intensity, the electromotive force arising from the induction of the current on itself is different in different parts of the section of the wire, being in general a function of the distance from the axis of the wire as well as of the time.” J. J. Thomson, who edited the third edition of Maxwell’s Treatise, states in a related footnote to paragraph 690 [23] of the Treatise, the following:

The inertia of the system, in accordance with a general law of dynamics, makes the current tend to distribute itself so that while fulfilling the condition that the whole flow across any cross section is given, the Kinetic Energy is as small as possible; and this tendency gets more and more powerful as the rapidity with which the momentum of the systems is reversed is increased.

This is the fundamental definition of what would later become known as the skin effect.

The skin effect is central to any discussions focused on plated conductors that are to be used for applications in which the operating frequency is above a few hundred kilohertz, and governs conductor impedance, in particular the resistance, as the operating frequency increases.

O. Heaviside [24-26] made a significant contribution with his work on the subject of skin effect from 1884 to 1887. In 1886, Lord Rayleigh [27] gave the first formula for

skin effect in an infinitely wide strip. Lord Kelvin [28] provided an expression in the now well-known ber, bei and ker, kei functions.

Jumping ahead a few years, in 1910, F. F. Fowle [29-31] wrote a series of three articles on the electrical properties of compound wires, a compound wire being one that has a solid core of one type of metal, and an outer layer of a different type of metal, in essence the forerunners of today's plated wires. In this series, Fowle referred to the skin effect as the dominating factor of concern for telephonic frequencies. He goes on to state that he does not attempt to account for skin effect in his work, but mentions that ratios of true to apparent resistance values would appear from measurement results presented later in the series, a direct allusion to the skin effect phenomenon. Fowle focused on copper clad steel conductors used in power distribution systems, and was able to develop a number of relationships between the relative weights of compound wires, the ratio of the conductance of a compound wire to that of a solid copper wire of the same diameter, and eventually derives an expression for the total internal inductance of a compound wire. Fowle does show some comparisons to measurements of relatively large conductors, and makes the key statement that his work is not applicable to compound wires comprising magnetic materials placed in close proximity one to the other.

Shortly after Fowle's papers were released, a series of about 100 experiments were undertaken at M.I.T.[32] to investigate skin effect in conductors. In this work, three definitions are provided: 1) a redistribution of current in a conductor caused by alternating magnetic flux, named as skin effect; 2) a reactance effect causing current redistribution in spiral wound stranded conductors, named as spirality; and 3) a redistribution of current in parallel linear conductors caused by an alternating magnetic flux emanating from one and penetrating the other, named the proximity effect. Experiments were conducted on copper and aluminum conductors in several configurations, including loops of solid round

conductors, stranded conductors, strip (flat) conductors, and tubular conductors.

Appendix 2 of the work provides an abbreviated exposition on Bessel functions of the first and second kind, and shows detailed calculations employing Bessel functions regarding the current distribution in the various conductors examined. The appendix also contains a section on the determination of the impedance ratio and the propagation constant for a stranded wire as compared to a solid conductor of equal cross-sectional area. The work concludes with an extensive bibliography of skin effect research to date at the time of publication.

H. B. Dwight, in two papers [33,34] discussed improved calculations for skin effect in tubular conductors, and proximity effect in several configurations of conductors, notably two parallel finite wire conductors, showing conclusively the manner in which the current is redistributed in such a configuration, and the impact to the resistance of the wire pair. Dwight employs Bessel functions in the ber, bei, and ker, kei form throughout the first paper, but then falls back on more standard Bessel forms for the second effort.

Improved formulae for the ac resistance of both solid and hollow round conductors, as well as for determination of proximity effects, were developed by A. H. M. Arnold in a 1941 paper [35]. The formulae employ Bessel functions and are shown to be very close in agreement to measured data from previous efforts.

A number of other papers have been published since 1941 on the topic of skin effect, but most of them leverage the previously listed works, and so are not included here, as they had less of an impact on this work.

## 2.2 Layered or coated conductors

In 1934, in a paper in the Bell Technical Journal [36], S. A. Schelkunoff shows that the surface impedance of a compound conductor can be expressed as a reduction formula using the transfer impedances that exist between each successive layer. The

relationships he derives are equally useful for determining the variation in internal impedance, as well as the distribution of currents inside the various layers of the compound conductor. Notably, Schelkunoff does not make use of Bessel functions for his expressions.

Then, in 1963, a seminal paper [37] is published, detailing for the first time an analysis of a copper conductor having a nickel coating. The analysis is founded on Maxwell's equations for the curl of E and H in the conductor, and makes extensive use of Bessel functions for the solution. The process is directly extensible to multiple layers of coatings. A very important observation is made in the latter part of the document with regard to the variability of the permeability of nickel as a function of field strength, and this places a restriction on the validity of the approach in terms of the amount of current that can be allowed to flow in the conductor. Another observation is that if the coating layer exceeds 10% of the total radius, the impedance of the compound conductor may depend sharply on the conductor current or on externally applied magnetic fields, and that such effects may be more marked than for a homogeneous nickel conductor. The paper goes on to state that at frequencies greater than about 1 MHz, the compound conductor operates essentially as a tubular nickel conductor. Thus the coating dominates the impedance of the compound conductor at frequencies greater than 1 MHz.

A few years later, another very interesting paper by A. M. Fowler [38] was published that documented a very thorough investigation into the characteristics of electroplated finishes on copper conductors. This paper talks directly about the distribution of electrical current inside a plated conductor, and speaks at length regarding the many issues surrounding various plating materials such as silver and nickel. Fowler discusses the fact that commercial plating processes incorporate numerous different brightening or grain-refining agents that act to diminish the conductivity of the plating

material, and that this is well documented in plating literature. He also points out that this is not well known by electrical or electronics engineers. But the problem goes even deeper, in that on the electroplaters' part, they believe the increase in conductivity is of no practical concern. Fowler employs Astbury's work from his 1963 paper to calculate the ac resistance and reactance behavior of several configurations of conductors and platings at the operating frequency of 10 MHz. In one case, he is able to show that the use of nickel plating can lead to very high radio frequency losses, depending on the thickness and the permeability of the plating layer. Fowler discusses the fact that very little information is available in the published literature on the conductivity of electro-deposited metals, and goes on to indicate that most efforts to measure the conductivity had up to that time been focused primarily on the determination of the presence of impurities, reports of which showed very wide variations. Perhaps most importantly, Fowler lists six specific actions that he felt should be undertaken to address the issue of uncontrolled electrical behavior of electro-plated finishes on conductors, to wit:

- 1) Education of electronic engineers in the basic properties of electro-deposits, and in the proper selection and specification of wire plating using the same care as used for any other component in the subsystem or system
- 2) Education of electroplaters in the problems of the electronics industry to ensure adherence to wire plating systems most commensurate to use by the electronics industry
- 3) Determination of the requirements of wire platings for the electronics industry
- 4) Revision of standards and specification for electro-plating to include sections on the electrical requirements of the wire plating
- 5) Development of suitable wire plating systems to meet the electronic industry's requirements, and finally

- 6) Development of suitable test methods and procedures to allow verification of the performance of plated wire in its intended operational radio frequency environment

Fowler includes an appendix in which he shows his implementation of Astbury's work, and also includes an extensive bibliography of published works addressing electroplating processes, measurements, difficulties, and applications pertinent to the electrical and electronic industries.

A more recent, and equally interesting paper published in 2009 by T. Graf et al [39], explores the magnetic behavior of a nickel plated 80  $\mu\text{m}$  diameter copper conductor, equivalent to a 40 AWG wire. The nickel coating thickness is 1.5  $\mu\text{m}$ , equivalent to a 7% coating thickness per ASTM B355-1 [5], somewhat heavier than the 2% more generally used in electrical, electronic, and aerospace applications. Figure 2-1 is a copy of Figure 1 from the Graf paper, illustrating a cross section view of the copper wire core and the nickel plating layer used in subsequent measurements.

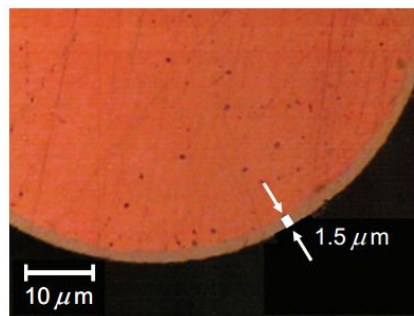


Figure 2-1 Cross section of Cu core with Ni layer [39]

Graf shows with both simulation and with measurements that the quality factor, or Q, of loops of nickel plated wire is dependent on the plating layer thickness, and concludes that the Q can be tuned by variation of the plating thickness, possibly finding application in



power transfer by magnetic resonance [40]. Graf also indicates the permeability of the nickel coating varies with frequency above 10 MHz.

## Chapter 3

### Foundational Theory

To begin the study of coated wires, it is appropriate to first examine the basic relationships that describe the current density and impedance of a solid, homogeneous, cylindrical conductor. With those basics established, a plating layer is introduced, and the impact to the basic theory will be explored. The interest in this paper is in long cylindrical conductors so the relationships will be developed in the cylindrical coordinate system for convenience and clarity. Much of the development of the material in this chapter relies heavily on the references cited in the previous chapter, a number of Bessel function references that proved extremely helpful [41-47], and a variety of commonly available sources available in text form by authors such as Cheng [48], King [49], Ramo, Whinnery & Van Duzer [50], Stratton [51], and Smythe [52].

#### 3.1 Solid homogeneous cylindrical conductors

##### 3.1.1. Current density

Consider a solid, homogeneous, infinitely long cylindrical conductor of radius  $a$ , as shown in Figure 3-1, whose axis is coincident with the  $z$ -axis of a cylindrical coordinate system.

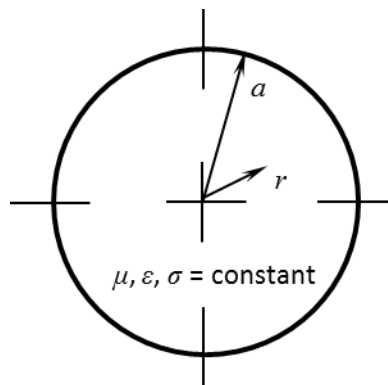


Figure 3-1 Cross section of cylindrical conductor

The permeability,  $\mu$ , the permittivity,  $\epsilon$ , and the conductivity,  $\sigma$ , of the conductor are constant throughout, and the net charge density,  $\rho$ , inside the conductor is zero. The permittivity is assumed to be that of free space.

The conductor is provided a time-domain current from a source whose output is defined as

$$i(t) = I_0 e^{j\omega t} \quad (1)$$

where  $I_0$  is the phasor current.

The current is only a function of time, and is steady otherwise. The conductor itself is assumed to have the characteristic

$$\omega\epsilon \ll \sigma \quad (2)$$

so that it is possible to ignore any displacement currents.

Everywhere in the conductor, the electromagnetic fields are described by the following relationships:

$$\nabla \times \bar{E}_z = -j\omega\mu\bar{H}_\phi \quad (3)$$

$$\nabla \times \bar{H}_\phi = \bar{J}_z \quad (4)$$

$$\nabla \cdot \bar{E} = 0 \quad (5)$$

$$\nabla \cdot \bar{H} = 0 \quad (6)$$

$$\bar{J}_z = \sigma\bar{E}_z \quad (7)$$

With the electromagnetic fields thus described, it is now possible to derive a differential relationship that describes the current density as a function of position inside the conductor. Taking the curl of (3)

$$\nabla \times \nabla \times \bar{E}_z = -j\omega\mu(\nabla \times \bar{H}_\phi) \quad (8)$$

then substituting (4) and (7) yields

$$\nabla \times \nabla \times \bar{J}_z = -j\omega\mu\sigma(\bar{J}_z) \quad (9)$$

$$\equiv \nabla(\nabla \cdot \bar{J}_z) - \nabla^2 \bar{J}_z \quad (10)$$

The divergence of  $J_z$  in the second expression is identically equal to zero, so that

$$\nabla^2 \bar{J}_z = j\omega\mu\sigma(J_z) \quad (11)$$

Recognizing that the current density is not a function of  $z$  or  $\varphi$ , the left hand side of (11) can then be expressed as a partial differential

$$\nabla^2 \bar{J}_z = \frac{1}{r} \frac{\partial}{\partial r} \left( r \frac{\partial J_z}{\partial r} \right) \quad (12)$$

so that 
$$\frac{\partial^2 J_z}{\partial r^2} + \frac{1}{r} \frac{\partial J_z}{\partial r} - (k^2 r \sqrt{j}) J_z = \frac{\partial^2 J_z}{\partial(\xi)^2} + \frac{1}{\xi} \frac{\partial J_z}{\partial(\xi)} - J_z = 0 \quad (13)$$

where 
$$k^2 = \omega\mu\sigma; \quad k = \sqrt{\omega\mu\sigma}; \quad \xi = kr\sqrt{j} \quad (0 \leq r \leq a) \quad (14)$$

Equation (13) is a Bessel equation. In general, this equation has two solutions, expressed in general form as

$$J_z(z) = C_1 I_\nu(z) + D_1 K_\nu(z) \quad (15)$$

where  $C_1$  and  $D_1$  are arbitrary constants, and  $I_\nu(z)$  and  $K_\nu(z)$  are known as modified Bessel functions of the first and second kind, respectively.

The modified Bessel function of the first kind is equal to one when the argument equals zero for all real values of  $z$ . The modified Bessel function of the second kind is singular when the argument is equal to zero for all real values of  $z$ . Since  $J_z$  in this case is finite at  $r = 0$ ,  $D_1$  must be equal to zero because  $K_\nu(z)$  is discontinuous at the origin.

The remaining solution for  $J_z(z)$  that is finite at  $r = 0$  may be expressed as an infinite series

$$J_z(z) = C_1 \left[ 1 + \left(\frac{z^2}{4}\right) \left(\frac{1}{1!}\right)^2 + \left(\frac{z^2}{4}\right)^2 \left(\frac{1}{2!}\right)^2 + \left(\frac{z^2}{4}\right)^3 \left(\frac{1}{3!}\right)^2 + \dots \right] \quad (16)$$

Equation (16) describes a modified Bessel function of the first kind, zeroth order. The general series expression for a modified Bessel function of the first kind, of any order, is given by

$$I_\nu(z) = \left(\frac{z}{2}\right)^\nu \sum_{k=0}^{\infty} \left(\frac{1}{k!}\right) \left[\frac{1}{(k+\nu)!}\right] \left(\frac{z^2}{4}\right)^k \quad (17)$$

The constant  $C_1$  in (16) can be evaluated simply by setting the current density equal to that at the surface of the cylindrical conductor.

$$J_z(ka\sqrt{j}) = C_1 I_0(ka\sqrt{j}) = \sigma E_0 \xrightarrow{\text{yields}} C_1 = \frac{\sigma E_0}{I_0(ka\sqrt{j})} \quad (18)$$

so that the current density everywhere in the solid, homogeneous, cylindrical conductor is then given by

$$J_z(z) = \frac{\sigma E_0 I_0(kr\sqrt{j})}{I_0(ka\sqrt{j})} \quad (19)$$

In general, the current density is not known *a priori*, but the total current is. It is therefore useful to express (19) in terms of the total current.

$$I_z = \iint J_z \cdot ds = \int_0^{2\pi} \int_0^a \frac{\sigma E_0 I_0(kr\sqrt{j})}{I_0(ka\sqrt{j})} \cdot r dr d\phi \quad (22)$$

$$= \frac{\sigma E_0}{I_0(ka\sqrt{j})} \int_0^{2\pi} \int_0^a I_0(kr\sqrt{j}) \cdot r dr d\phi \quad (23)$$

$$= \frac{2\pi\sigma E_0}{I_0(ka\sqrt{j})} \int_0^a I_0(kr\sqrt{j}) \cdot r dr \quad (24)$$

Let  $kr\sqrt{j} = x$ . Then if  $r = 0, x = 0$ , and when  $r = a, x = ka\sqrt{j}$ , and  $dr = \frac{dx}{k\sqrt{j}}$ . With this

change of variable, (24) becomes

$$I_z = \frac{2\pi\sigma E_0}{I_0(ka\sqrt{j})} \int_0^{ka\sqrt{j}} \frac{1}{jk^2} I_0(x) \cdot x dx \quad (25)$$

Using the relationship

$$\int z^{\nu+1} I_\nu(z) dz = z^{\nu+1} I_{\nu+1}(z) \quad (26)$$

equation (25) becomes

$$I_z = \frac{2\pi\sigma a E_0}{k\sqrt{j}} \frac{I_1(ka\sqrt{j})}{I_0(ka\sqrt{j})} \quad (27)$$

### 3.1.2. Impedance

Building on the previous section, the impedance of cylindrical conductors can be determined. The voltage on the cylindrical conductor of length  $l$  is found as

$$V = - \int_a^b E \cdot dl = - \int_l^0 E_0 \cdot dz = E_0 l \quad (28)$$

Using (27), the impedance per unit length is then given by

$$Z_l = \frac{E_0 l}{I l} = \frac{E_0}{\frac{2\pi\sigma a E_0 I_1(ka\sqrt{j})}{k\sqrt{j}} I_0(ka\sqrt{j})} = \frac{k\sqrt{j} I_0(ka\sqrt{j})}{2\pi\sigma a I_1(ka\sqrt{j})} \quad (29)$$

Using the definitions

$$I_0(ka\sqrt{j}) = \text{ber } ka + j \text{ bei } ka ; I_1(ka\sqrt{j}) = I_0'(ka\sqrt{j}) = (j)^{-1/2} (\text{ber}' ka + j \text{ bei}' ka) \quad (30)$$

equation (29) becomes

$$Z_l = \frac{k}{2\pi\sigma a} \frac{(-\text{bei } ka + j \text{ ber } ka)}{(\text{ber}' ka + j \text{ bei}' ka)} \quad (31)$$

Using series expansions of the ber and bei functions, approximations can be made for both small and large values of  $(ka)$ .

For small values of  $(ka)$ , the ber, ber', bei, and bei' functions may be expressed as series expansions, shown as follows:

$$\text{ber } z = \left[ 1 - \frac{(z)^4}{64} + \dots \right] \quad (32)$$

$$\text{bei } z = \left[ \frac{(z)^2}{4} - \frac{(z)^6}{2304} + \dots \right] \quad (33)$$

$$\text{ber}' z = \left[ -\frac{(z)^3}{16} + \frac{(z)^7}{18432} - \dots \right] \quad (34)$$

$$\text{bei}' z = \left[ \frac{z}{2} - \frac{(z)^5}{384} + \dots \right] \quad (35)$$

Discarding higher order terms and substituting (32) through (35) into (31) yields

$$Z_l = \frac{k}{2\pi\sigma a} \frac{\left( -\frac{(ka)^2}{4} + j \right)}{\left( -\frac{(ka)^3}{16} + j \frac{ka}{2} \right)} \quad (36)$$

Simplifying, and dropping terms of  $(ka)^4$  and greater yields the low frequency approximation for the impedance of a solid cylindrical conductor

$$Z_l \approx \frac{1}{\pi\sigma a^2} \left[ 1 + j \frac{(ka)^2}{8} \right] = \frac{1}{\pi\sigma a^2} + j \frac{\omega\mu}{8\pi} \quad (37)$$

The left-hand term on the right side is the dc resistance of the cylindrical conductor. The right-most term is the internal inductance of the cylindrical conductor. This term is a constant dependent only on the permeability of the conductor material.

For large values of  $(ka)$ , it becomes necessary to use asymptotic expressions for the ber, ber', bei, and bei' functions, given by

$$\text{ber } z + j \text{bei } z = \frac{1}{\sqrt{2\pi z}} \exp \left[ \frac{z}{\sqrt{2}} + j \left( \frac{z}{\sqrt{2}} - \frac{\pi}{8} \right) \right] \quad (38)$$

$$-\text{bei } z + j \text{ber}' z = \frac{1}{\sqrt{2\pi z}} \exp \left[ \frac{z}{\sqrt{2}} + j \left( \frac{z}{\sqrt{2}} + \frac{\pi}{8} \right) \right] \quad (39)$$

Starting from (31) as was done previously for the small argument case, and substituting (38) and (39) yields

$$Z_l \sim \frac{k}{2\pi\sigma a} \frac{\frac{1}{\sqrt{2\pi z}} \exp \left[ \frac{z}{\sqrt{2}} + j \left( \frac{z}{\sqrt{2}} + \frac{\pi}{8} \right) \right]}{\frac{1}{\sqrt{2\pi z}} \exp \left[ \frac{z}{\sqrt{2}} + j \left( \frac{z}{\sqrt{2}} - \frac{\pi}{8} \right) \right]} = \frac{k}{2\pi\sigma a} e^{j\pi/4} \quad (40)$$

Thus, the high frequency approximation for the impedance per unit length of a solid cylindrical conductor is

$$Z_l \sim \frac{(1+j)}{2\pi a} \sqrt{\frac{\omega\mu}{2\sigma}} \quad (41)$$

## 3.2 Solid cylindrical conductors with plating layers

### 3.2.1. Current density

Consider now the same solid, homogeneous, infinitely long cylindrical conductor of radius  $a$ , as was shown in Figure 3-1, with one or more plating layers of conductive material of different permeability,  $\mu$ , permittivity,  $\epsilon$ , and conductivity,  $\sigma$ , than that of the core conductor. Figure 3-2 is a depiction of this arrangement for a core of radius  $a$ , and a single plating layer, with inner radius  $a$ , and outer radius  $b$ . In the core, and in each

successive plating layer, the permeability,  $\mu$ , permittivity,  $\epsilon$ , and conductivity,  $\sigma$ , may be different according to the conductive material constitutive parameters, but throughout each type of conductive material the constitutive parameters are constant. The net charge densities,  $\rho$ , everywhere inside the core and the layers, are zero. The permittivity throughout is assumed to be that of free space. The current density in the core and each successive plating layer is still described by some combination of Bessel functions, the argument  $w$  being dependent for each solution on the constitutive parameters for the conductive material of the core or layer under consideration. Development will proceed here assuming a configuration of a core and a single layer.

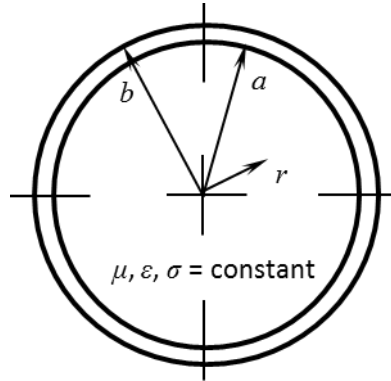


Figure 3-2 Cross section of a cylindrical conductor with a single plating layer

Referring to Figure 3-2, the same conditions apply in the core (layer 1) as previously discussed in section 3.1, so the solution is given by

$$J_{z1}(\xi_1) = C_1 I_0(\xi_1) + D_1 K_0(\xi_1); \quad 0 \leq r \leq a \quad (42)$$

where  $k_1^2 = \omega\mu_1\sigma_1$ ,  $k_1 = \sqrt{\omega\mu_1\sigma_1}$ ,  $\xi_1 = k_1 r \sqrt{j}$ ,  $C_1$  and  $D_1$  are arbitrary constants, and  $I_0(w_1)$  and  $K_0(w_1)$  are Bessel functions of the first and second kind, respectively.

For the plating layer, the solution is given by

$$J_{z2}(\xi_2) = C_2 I_0(\xi_2) + D_2 K_0(\xi_2); \quad a \leq r \leq b \quad (43)$$

where  $k_2^2 = \omega\mu_2\sigma_2$ ,  $k_2 = \sqrt{\omega\mu_2\sigma_2}$ ,  $\xi_2 = k_2 r \sqrt{j}$ ,  $C_2$  and  $D_2$  are arbitrary constants.



Since  $J_z$  in this case is finite at  $r = 0$ ,  $D_1$  must be equal to zero because  $K_\nu(z)$  is discontinuous at the origin. So (42) becomes

$$J_{z1}(\xi_1) = C_1 I_0(\xi_1); \quad 0 \leq r \leq a \quad (44)$$

The remaining constants must be determined by the following conditions:

$$\bar{E}_{z1a} = \bar{E}_{z2a}; \quad r = a \quad (45)$$

$$\bar{H}_{\phi 1a} = \bar{H}_{\phi 2a}; \quad r = a \quad (46)$$

$$\bar{J}_{z2b} = \bar{J}_{z0} = \sigma_2 \bar{E}_{z0}; \quad r = b \quad (47)$$

where  $\bar{J}_{z0}$  is the current density on the surface of the plating layer, and  $\bar{E}_{z0}$  is the z-component of the electric field intensity at the surface of the plating layer.

Equation (45) can be rewritten in terms of  $\bar{J}_z$  as

$$\frac{\bar{J}_{z1a}}{\sigma_1} = \frac{\bar{J}_{z2a}}{\sigma_2}; \quad r = a \quad (48)$$

Using (3), and recognizing that  $\nabla \times \bar{J} = -\frac{\partial J_z}{\partial r}$ , equation (46) can be rewritten in terms of  $\bar{J}_z$  as

$$\frac{r}{\xi_1} \frac{\partial J_{z1a}}{\partial \xi_1} = \frac{r}{\xi_2} \frac{\partial J_{z2a}}{\partial \xi_2}; \quad r = a \quad (49)$$

Using (45) through (49), the following relationships involving (43) and (44) result:

$$\frac{C_1 I_0(\xi_{1a})}{\sigma_1} = \frac{C_2 I_0(\xi_{2a})}{\sigma_2} + \frac{D_2 K_0(\xi_{2a})}{\sigma_2}; \quad r = a \quad (50)$$

$$\frac{C_1 I_0'(\xi_{1a})}{\xi_{1a}} = \frac{C_2 I_0'(\xi_{2a})}{\xi_{2a}} + \frac{D_2 K_0'(\xi_{2a})}{\xi_{2a}}; \quad r = a \quad (51)$$

$$J_{z0} = C_2 I_0(\xi_{2b}) + D_2 K_0(\xi_{2b}); \quad r = b \quad (52)$$

where the terms  $\xi_{1a}$ ,  $\xi_{2a}$ , and  $\xi_{2b}$  refer to the argument  $\xi$  as appropriate for the core or plating layer, evaluated at the radius  $a$  or  $b$ .

Using the derivative relationships

$$I_0'(z) = I_1(z) \quad \text{and} \quad K_0'(z) = -K_1(z) \quad (53)$$

equations (50) through (52) compose a system of three simultaneous equations in three unknowns, and can therefore be formed into matrix and vector relationships

$$\begin{bmatrix} \frac{I_0(\xi_{1a})}{\sigma_1} & \frac{-I_0(\xi_{2a})}{\sigma_2} & \frac{-K_0(\xi_{2a})}{\sigma_2} \\ I_1(\xi_{1a}) & -I_1(\xi_{2a}) & K_1(\xi_{2a}) \\ \xi_{1a} & \xi_{2a} & \xi_{2a} \\ 0 & I_0(\xi_{2b}) & K_0(\xi_{2b}) \end{bmatrix} \begin{bmatrix} C_1 \\ C_2 \\ D_2 \end{bmatrix} = \begin{bmatrix} 0 \\ 0 \\ J_{z0} \end{bmatrix} \quad (54)$$

The determinant of (54) is given by

$$\begin{aligned} Det = I_0(\xi_{2b}) & \left\{ \left[ \frac{-K_0(\xi_{2a})}{\sigma_2} \right] \left[ \frac{I_1(\xi_{1a})}{\xi_{1a}} \right] - \left[ \frac{I_0(\xi_{1a})}{\sigma_1} \right] \left[ \frac{K_1(\xi_{2a})}{\xi_{2a}} \right] \right\} \\ & + K_0(\xi_{2b}) \left\{ \left[ \frac{I_0(\xi_{1a})}{\sigma_1} \right] \left[ \frac{-I_1(\xi_{2a})}{\xi_{2a}} \right] - \left[ \frac{-I_0(\xi_{2a})}{\sigma_2} \right] \left[ \frac{I_1(\xi_{1a})}{\xi_{1a}} \right] \right\} \end{aligned} \quad (55)$$

Using Cramer's Rule, each of the three constants may be found by replacing the corresponding column in the matrix with the RHS column vector. Using this approach, the matrix to solve for  $C_1$  is given by

$$\begin{bmatrix} 0 & \frac{-I_0(\xi_{2a})}{\sigma_2} & \frac{-K_0(\xi_{2a})}{\sigma_2} \\ 0 & \frac{-I_1(\xi_{2a})}{\xi_{2a}} & \frac{K_1(\xi_{2a})}{\xi_{2a}} \\ J_{z0} & I_0(\xi_{2b}) & K_0(\xi_{2b}) \end{bmatrix} \quad (56)$$

and the determinant of this matrix is

$$Det_{C_1} = J_{z0} \left[ \left( \frac{-I_0(\xi_{2a})}{\sigma_2} \right) \left( \frac{K_1(\xi_{2a})}{\xi_{2a}} \right) - \left( \frac{-K_0(\xi_{2a})}{\sigma_2} \right) \left( \frac{-I_1(\xi_{2a})}{\xi_{2a}} \right) \right] \quad (57)$$

Then, by Cramer's Rule,

$$C_1 = \frac{Det_{C_1}}{Det} \quad (58)$$

$$\begin{aligned} & \frac{J_{z0} \left[ \left( \frac{-I_0(\xi_{2a})}{\sigma_2} \right) \left( \frac{K_1(\xi_{2a})}{\xi_{2a}} \right) - \left( \frac{-K_0(\xi_{2a})}{\sigma_2} \right) \left( \frac{-I_1(\xi_{2a})}{\xi_{2a}} \right) \right]}{I_0(\xi_{2b}) \left\{ \frac{-K_0(\xi_{2a})}{\sigma_2} \frac{I_1(\xi_{1a})}{\xi_{1a}} - \frac{I_0(\xi_{1a})}{\sigma_1} \frac{K_1(\xi_{2a})}{\xi_{2a}} \right\} + K_0(\xi_{2b}) \left\{ \frac{-I_1(\xi_{2a})}{\xi_{2a}} \frac{I_0(\xi_{1a})}{\sigma_1} + \frac{I_0(\xi_{2a})}{\sigma_2} \frac{I_1(\xi_{1a})}{\xi_{1a}} \right\}} \end{aligned}$$

In entirely similar fashion, the remaining two constants are given by

$$C_2 = \frac{Det_{C_2}}{Det} \quad (59)$$

$$= \frac{J_{z0} \left[ \frac{-K_0(\xi_{2a}) I_1(\xi_{1a})}{\sigma_2 \xi_{1a}} - \frac{I_0(\xi_{1a}) K_1(\xi_{2a})}{\sigma_1 \xi_{2a}} \right]}{I_0(\xi_{2b}) \left\{ \frac{-K_0(\xi_{2a}) I_1(\xi_{1a})}{\sigma_2 \xi_{1a}} - \frac{I_0(\xi_{1a}) K_1(\xi_{2a})}{\sigma_1 \xi_{2a}} \right\} + K_0(\xi_{2b}) \left\{ \frac{-I_1(\xi_{2a}) I_0(\xi_{1a})}{\xi_{2a} \sigma_1} + \frac{I_0(\xi_{2a}) I_1(\xi_{1a})}{\sigma_2 \xi_{1a}} \right\}}$$

$$D_2 = \frac{Det_{D_2}}{Det} \quad (60)$$

$$= \frac{J_{z0} \left[ \frac{-I_1(\xi_{2a}) I_0(\xi_{1a})}{\xi_{2a} \sigma_1} - \frac{-I_0(\xi_{2a}) I_1(\xi_{1a})}{\sigma_2 \xi_{1a}} \right]}{I_0(\xi_{2b}) \left\{ \frac{-K_0(\xi_{2a}) I_1(\xi_{1a})}{\sigma_2 \xi_{1a}} - \frac{I_0(\xi_{1a}) K_1(\xi_{2a})}{\sigma_1 \xi_{2a}} \right\} + K_0(\xi_{2b}) \left\{ \frac{-I_1(\xi_{2a}) I_0(\xi_{1a})}{\xi_{2a} \sigma_1} + \frac{I_0(\xi_{2a}) I_1(\xi_{1a})}{\sigma_2 \xi_{1a}} \right\}}$$

Substituting (58) into (44) yields

$$J_{z1}(\xi_1) = I_0(\xi_1) \frac{J_{z0} \left[ \frac{(-I_0(\xi_{2a})) (K_1(\xi_{2a}))}{\sigma_2 \xi_{2a}} - \frac{(K_0(\xi_{2a})) (I_1(\xi_{2a}))}{\sigma_2 \xi_{2a}} \right]}{I_0(\xi_{2b}) \left\{ \frac{-K_0(\xi_{2a}) I_1(\xi_{1a})}{\sigma_2 \xi_{1a}} - \frac{I_0(\xi_{1a}) K_1(\xi_{2a})}{\sigma_1 \xi_{2a}} \right\} + K_0(\xi_{2b}) \left\{ \frac{-I_1(\xi_{2a}) I_0(\xi_{1a})}{\xi_{2a} \sigma_1} + \frac{I_0(\xi_{2a}) I_1(\xi_{1a})}{\sigma_2 \xi_{1a}} \right\}} \quad (61)$$

which is a complete expression for the current density in the core for  $0 \leq r \leq a$ .

Substituting (59) and (60) into (43) yields

$$J_{z2}(\xi_2) = I_0(\xi_2) \frac{J_{z0} \left[ \frac{-K_0(\xi_{2a}) I_1(\xi_{1a})}{\sigma_2 \xi_{1a}} - \frac{I_0(\xi_{1a}) K_1(\xi_{2a})}{\sigma_1 \xi_{2a}} \right]}{I_0(\xi_{2b}) \left\{ \frac{-K_0(\xi_{2a}) I_1(\xi_{1a})}{\sigma_2 \xi_{1a}} - \frac{I_0(\xi_{1a}) K_1(\xi_{2a})}{\sigma_1 \xi_{2a}} \right\} + K_0(\xi_{2b}) \left\{ \frac{-I_1(\xi_{2a}) I_0(\xi_{1a})}{\xi_{2a} \sigma_1} + \frac{I_0(\xi_{2a}) I_1(\xi_{1a})}{\sigma_2 \xi_{1a}} \right\}}$$

$$+ K_0(\xi_2) \frac{J_{z0} \left[ \frac{-I_1(\xi_{2a}) I_0(\xi_{1a})}{\xi_{2a} \sigma_1} - \frac{-I_0(\xi_{2a}) I_1(\xi_{1a})}{\sigma_2 \xi_{1a}} \right]}{I_0(\xi_{2b}) \left\{ \frac{-K_0(\xi_{2a}) I_1(\xi_{1a})}{\sigma_2 \xi_{1a}} - \frac{I_0(\xi_{1a}) K_1(\xi_{2a})}{\sigma_1 \xi_{2a}} \right\} + K_0(\xi_{2b}) \left\{ \frac{-I_1(\xi_{2a}) I_0(\xi_{1a})}{\xi_{2a} \sigma_1} + \frac{I_0(\xi_{2a}) I_1(\xi_{1a})}{\sigma_2 \xi_{1a}} \right\}} \quad (62)$$

which is a complete expression for the current density in the plating layer for  $a \leq r \leq b$ .

As a check on the foregoing derivation, if the conductor were solid and homogeneous, as in section 3.1, (61) should reduce to (19) with the proper substitutions. Since there would be only the core material, or material 1, all  $\xi_{2a}$  terms should be replaced by  $\xi_{1a}$  terms. Also, all  $\sigma_2$  terms should be replaced with  $\sigma_1$  terms. The  $\xi_{2b}$  terms should be replaced with  $\xi_{1a}$  terms. With these substitutions, (74) becomes

$$J_{z1}(\xi_1) = I_0(\xi_1) \frac{J_{z0} \left[ \frac{(-I_0(\xi_{1a})) (K_1(\xi_{1a}))}{\sigma_1 \xi_{1a}} - \frac{(K_0(\xi_{1a})) (I_1(\xi_{1a}))}{\sigma_1 \xi_{1a}} \right]}{I_0(\xi_{1a}) \left\{ \frac{-K_0(\xi_{1a}) I_1(\xi_{1a})}{\sigma_1 \xi_{1a}} - \frac{I_0(\xi_{1a}) K_1(\xi_{1a})}{\sigma_1 \xi_{1a}} \right\} + K_0(\xi_{1a}) \left\{ \frac{-I_1(\xi_{1a}) I_0(\xi_{1a})}{\xi_{1a} \sigma_1} + \frac{I_0(\xi_{1a}) I_1(\xi_{1a})}{\sigma_1 \xi_{1a}} \right\}} \quad (63)$$

$$J_{z1}(\xi_1) = \frac{\sigma_1 E_{z0} I_0(\xi_1)}{I_0(\xi_{1a})} = \frac{\sigma E_0 I_0(kr\sqrt{j})}{I_0(ka\sqrt{j})} \quad (64)$$

which is identical to (19), with  $J_{z1}(\xi_1) = J_z(z)$ ,  $\sigma_1 E_{z0} I_0(\xi_1) = \sigma E_0 I_0(kr\sqrt{j})$ , and

$$I_0(\xi_{1a}) = I_0(ka\sqrt{j}).$$

As was stated previously, the current density is generally unknown *a priori*, but the total current is known. The total current density distribution throughout the plated conductor can be expressed in terms of (61) and (62).

$$J_z = \begin{cases} J_{z1}(\xi_1); & (0 \leq r \leq a) \\ J_{z2}(\xi_2); & (a \leq r \leq b) \end{cases} \quad (65)$$

$$J_z = \begin{cases} I_0(\xi_1) \frac{J_{z0} \left[ \frac{(-I_0(\xi_{2a})) \left( \frac{K_1(\xi_{2a})}{\xi_{2a}} \right) - \left( \frac{K_0(\xi_{2a})}{\sigma_2} \right) \left( \frac{I_1(\xi_{2a})}{\xi_{2a}} \right) \right]}{I_0(\xi_{2b}) \left\{ \frac{-K_0(\xi_{2a}) I_1(\xi_{1a})}{\sigma_2 \xi_{1a}} - \frac{I_0(\xi_{1a}) K_1(\xi_{2a})}{\sigma_1 \xi_{2a}} \right\} + K_0(\xi_{2b}) \left\{ \frac{-I_1(\xi_{2a}) I_0(\xi_{1a})}{\xi_{2a} \sigma_1} + \frac{I_0(\xi_{2a}) I_1(\xi_{1a})}{\sigma_2 \xi_{1a}} \right\}}; & (0 \leq r \leq a) \\ I_0(\xi_2) \frac{J_{z0} \left[ \frac{-K_0(\xi_{2a}) I_1(\xi_{1a})}{\sigma_2 \xi_{1a}} - \frac{I_0(\xi_{1a}) K_1(\xi_{2a})}{\sigma_1 \xi_{2a}} \right]}{I_0(\xi_{2b}) \left\{ \frac{-K_0(\xi_{2a}) I_1(\xi_{1a})}{\sigma_2 \xi_{1a}} - \frac{I_0(\xi_{1a}) K_1(\xi_{2a})}{\sigma_1 \xi_{2a}} \right\} + K_0(\xi_{2b}) \left\{ \frac{-I_1(\xi_{2a}) I_0(\xi_{1a})}{\xi_{2a} \sigma_1} + \frac{I_0(\xi_{2a}) I_1(\xi_{1a})}{\sigma_2 \xi_{1a}} \right\}} \\ + K_0(\xi_2) \frac{J_{z0} \left[ \frac{-I_1(\xi_{2a}) I_0(\xi_{1a})}{\xi_{2a} \sigma_1} - \frac{-I_0(\xi_{2a}) I_1(\xi_{1a})}{\sigma_2 \xi_{1a}} \right]}{I_0(\xi_{2b}) \left\{ \frac{-K_0(\xi_{2a}) I_1(\xi_{1a})}{\sigma_2 \xi_{1a}} - \frac{I_0(\xi_{1a}) K_1(\xi_{2a})}{\sigma_1 \xi_{2a}} \right\} + K_0(\xi_{2b}) \left\{ \frac{-I_1(\xi_{2a}) I_0(\xi_{1a})}{\xi_{2a} \sigma_1} + \frac{I_0(\xi_{2a}) I_1(\xi_{1a})}{\sigma_2 \xi_{1a}} \right\}}; & (a \leq r \leq b) \end{cases} \quad (66)$$

It is useful to introduce some auxiliary variables here to shorten the expressions.

Recognizing that all terms that are a function of a fixed conductivity or radius are constants, they can each be assigned to auxiliary variables as follows:

$$c_1 = \frac{\left[ \frac{(-I_0(\xi_{2a})) \left( \frac{K_1(\xi_{2a})}{\xi_{2a}} \right) - \left( \frac{K_0(\xi_{2a})}{\sigma_2} \right) \left( \frac{I_1(\xi_{2a})}{\xi_{2a}} \right) \right]}{I_0(\xi_{2b}) \left\{ \frac{-K_0(\xi_{2a}) I_1(\xi_{1a})}{\sigma_2 \xi_{1a}} - \frac{I_0(\xi_{1a}) K_1(\xi_{2a})}{\sigma_1 \xi_{2a}} \right\} + K_0(\xi_{2b}) \left\{ \frac{-I_1(\xi_{2a}) I_0(\xi_{1a})}{\xi_{2a} \sigma_1} + \frac{I_0(\xi_{2a}) I_1(\xi_{1a})}{\sigma_2 \xi_{1a}} \right\}} \quad (67)$$

$$= \frac{-I_0(\xi_{2a}) K_1(\xi_{2a}) - K_0(\xi_{2a}) I_1(\xi_{2a})}{I_0(\xi_{2b}) \left\{ \sqrt{\frac{\mu_2 \sigma_2}{\mu_1 \sigma_1}} [-K_0(\xi_{2a})] I_1(\xi_{1a}) - \left( \frac{\sigma_2}{\sigma_1} \right) I_0(\xi_{1a}) K_1(\xi_{2a}) \right\} + K_0(\xi_{2b}) \left\{ \left( \frac{\sigma_2}{\sigma_1} \right) [-I_1(\xi_{2a})] I_0(\xi_{1a}) + \sqrt{\frac{\mu_2 \sigma_2}{\mu_1 \sigma_1}} I_0(\xi_{2a}) I_1(\xi_{1a}) \right\}}$$

$$c_{2a} = \frac{\left[ \frac{-K_0(\xi_{2a}) I_1(\xi_{1a})}{\sigma_2 \xi_{1a}} - \frac{I_0(\xi_{1a}) K_1(\xi_{2a})}{\sigma_1 \xi_{2a}} \right]}{I_0(\xi_{2b}) \left\{ \frac{-K_0(\xi_{2a}) I_1(\xi_{1a})}{\sigma_2 \xi_{1a}} - \frac{I_0(\xi_{1a}) K_1(\xi_{2a})}{\sigma_1 \xi_{2a}} \right\} + K_0(\xi_{2b}) \left\{ \frac{-I_1(\xi_{2a}) I_0(\xi_{1a})}{\xi_{2a} \sigma_1} + \frac{I_0(\xi_{2a}) I_1(\xi_{1a})}{\sigma_2 \xi_{1a}} \right\}} \quad (68)$$

$$= \frac{\sqrt{\frac{\mu_2 \sigma_2}{\mu_1 \sigma_1}} [-K_0(\xi_{2a})] I_1(\xi_{1a}) - \left( \frac{\sigma_2}{\sigma_1} \right) I_0(\xi_{1a}) K_1(\xi_{2a})}{I_0(\xi_{2b}) \left\{ \sqrt{\frac{\mu_2 \sigma_2}{\mu_1 \sigma_1}} [-K_0(\xi_{2a})] I_1(\xi_{1a}) - \left( \frac{\sigma_2}{\sigma_1} \right) I_0(\xi_{1a}) K_1(\xi_{2a}) \right\} + K_0(\xi_{2b}) \left\{ \left( \frac{\sigma_2}{\sigma_1} \right) [-I_1(\xi_{2a})] I_0(\xi_{1a}) + \sqrt{\frac{\mu_2 \sigma_2}{\mu_1 \sigma_1}} I_0(\xi_{2a}) I_1(\xi_{1a}) \right\}}$$

$$c_{2b} = \frac{\left[ \frac{-I_1(\xi_{2a}) I_0(\xi_{1a})}{\xi_{2a} \sigma_1} - \frac{-I_0(\xi_{2a}) I_1(\xi_{1a})}{\sigma_2 \xi_{1a}} \right]}{I_0(\xi_{2b}) \left\{ \frac{-K_0(\xi_{2a}) I_1(\xi_{1a})}{\sigma_2 \xi_{1a}} - \frac{I_0(\xi_{1a}) K_1(\xi_{2a})}{\sigma_1 \xi_{2a}} \right\} + K_0(\xi_{2b}) \left\{ \frac{-I_1(\xi_{2a}) I_0(\xi_{1a})}{\xi_{2a} \sigma_1} + \frac{I_0(\xi_{2a}) I_1(\xi_{1a})}{\sigma_2 \xi_{1a}} \right\}} \quad (69)$$

$$= \frac{\left(\frac{\sigma_2}{\sigma_1}\right)[-I_1(\xi_{2a})I_0(\xi_{1a}) + \sqrt{\frac{\mu_2\sigma_2}{\mu_1\sigma_1}}I_0(\xi_{2a})I_1(\xi_{1a})]}{I_0(\xi_{2b})\left\{\sqrt{\frac{\mu_2\sigma_2}{\mu_1\sigma_1}}-K_0(\xi_{2a})\right\}I_1(\xi_{1a}) - \left(\frac{\sigma_2}{\sigma_1}\right)I_0(\xi_{1a})K_1(\xi_{2a})} + K_0(\xi_{2b})\left\{\left(\frac{\sigma_2}{\sigma_1}\right)[-I_1(\xi_{2a})]I_0(\xi_{1a}) + \sqrt{\frac{\mu_2\sigma_2}{\mu_1\sigma_1}}I_0(\xi_{2a})I_1(\xi_{1a})\right\}$$

Equation (66) then becomes

$$J_z = \begin{cases} I_0(\xi_1)(\sigma_2 E_{z0} c_1); & (0 \leq r \leq a) \\ I_0(\xi_2)(\sigma_2 E_{z0} c_{2a}) + K_0(\xi_2)(\sigma_2 E_{z0} c_{2b}); & (a \leq r \leq b) \end{cases} \quad (70)$$

Proceeding as before with the solid homogeneous conductor, the total current can be expressed in terms of the current densities as

$$I_z = \iint J_z \cdot ds = \int_0^{2\pi} \int_0^a I_0(\xi_1)(\sigma_2 E_{z0} c_1) \cdot r dr d\varphi + \int_0^{2\pi} \int_a^b I_0(\xi_2)(\sigma_2 E_{z0} c_{2a}) \cdot r dr d\varphi + \int_0^{2\pi} \int_a^b K_0(\xi_2)(\sigma_2 E_{z0} c_{2b}) \cdot r dr d\varphi \quad (71)$$

$$= 2\pi\sigma_2 E_{z0} c_1 \int_0^a I_0(\xi_1) \cdot r dr + 2\pi\sigma_2 E_{z0} c_{2a} \int_a^b I_0(\xi_2) \cdot r dr + 2\pi\sigma_2 E_{z0} c_{2b} \int_a^b K_0(\xi_2) \cdot r dr \quad (72)$$

In the first term on the RHS, let  $k_1 r \sqrt{j} = x$ . Then if  $r = 0, x = 0$ , and when  $r = a, x =$

$k_1 a \sqrt{j}$ , and  $dr = \frac{dx}{k_1 \sqrt{j}}$ . In the second and third terms on the RHS, let  $k_2 r \sqrt{j} = x$ . Then if

$r = a, x = k_2 a \sqrt{j}$ , and when  $r = b, x = k_2 b \sqrt{j}$ , and  $dr = \frac{dx}{k_2 \sqrt{j}}$ . With these changes of

variable, (72) becomes

$$I_z = 2\pi\sigma_2 E_{z0} c_1 \int_0^{k_1 a \sqrt{j}} \frac{1}{jk_1^2} x I_0(x) \cdot dx + 2\pi\sigma_2 E_{z0} \int_{k_2 a \sqrt{j}}^{k_2 b \sqrt{j}} \frac{1}{jk_2^2} x [c_{2a} I_0(x) + c_{2b} K_0(x)] \cdot dx \quad (73)$$

Using the relationship given in (26), and using the relationships

$$\int x I_0(x) \cdot dx = x I_1(x); \int x K_0(x) \cdot dx = -x K_1(x) \quad (74)$$

equation (73) becomes

$$I_z = \frac{2\pi\sigma_2 a E_{z0} c_1}{k_1 \sqrt{j}} I_1(\xi_{1a}) + \frac{2\pi\sigma_2 E_{z0}}{k_2 \sqrt{j}} \{c_{2a} [b I_1(\xi_{2b}) - a I_1(\xi_{2a})] + c_{2b} [-b K_1(\xi_{2b}) + a K_1(\xi_{2a})]\} \quad (75)$$

### 3.2.2. Impedance

Building on the previous section, the impedance of a cylindrical conductor with a single plating layer can be determined. The voltage on the cylindrical conductor of length  $l$  is found as

$$V = - \int_a^b E \cdot dl = - \int_l^0 E_{z0} \cdot dz = E_{z0}l \quad (76)$$

Using (74), the impedance per unit length is then given by

$$Z_l = \frac{E_{z0}l}{I_zl} = \frac{1}{\frac{2\pi\sigma_2ac_1}{k_1\sqrt{j}}I_1(\xi_{1a}) + \frac{2\pi\sigma_2}{k_2\sqrt{j}}\{c_{2a}[bI_1(\xi_{2b}) - aI_1(\xi_{2a})] + c_{2b}[-bK_1(\xi_{2b}) + aK_1(\xi_{2a})]\}} \quad (77)$$

Unlike the previous case with equation (31), rather than attempt to simplify the expression, it is easier to simply solve equation (77) numerically, and plot the results for comparison. Shown in Fig. 3-3 are the data for the cases of pure metal wires, while shown in Fig. 3-4 are the data for copper wire plated with silver, tin, and nickel. The simulation used a 20 AWG nominal wire gage, and typical industry plating thicknesses of 40 μ-in, 40 μ-in, and 50 μ-in, respectively, for silver, tin, and nickel plating layers.

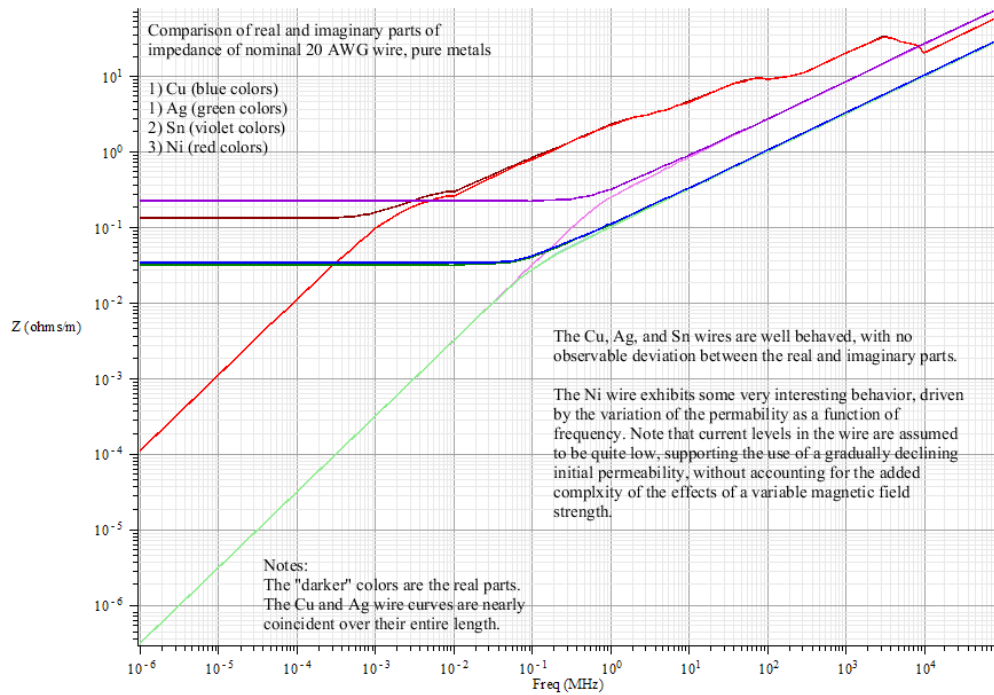


Figure 3-3 Impedance behavior of pure metals

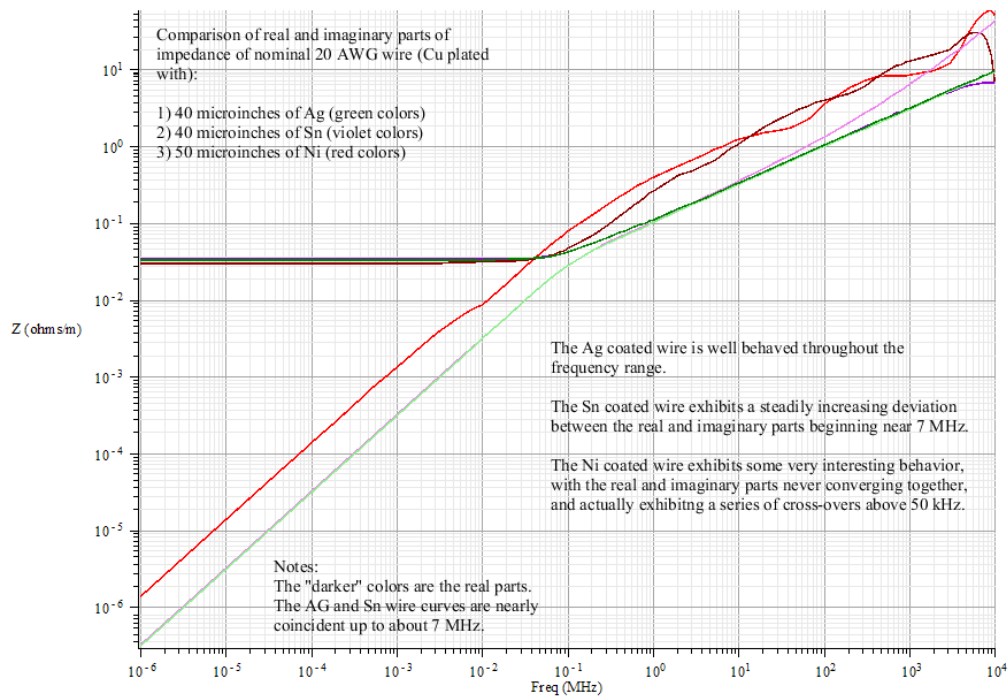


Figure 3-4 Impedance behavior of coated metals

It is necessary to mention at this point that the permeability of nickel is widely variable, and is a function of both ambient field strength and of frequency. For the purposes of completing a representative plot, a curve of the permeability of nickel as a function of frequency was developed from information gleaned from multiple sources [53-62], and is included for examination. This curve, shown in Fig. 3-5, was used as an input to the numerical routine used to plot the impedance behavior of the plated copper wire.

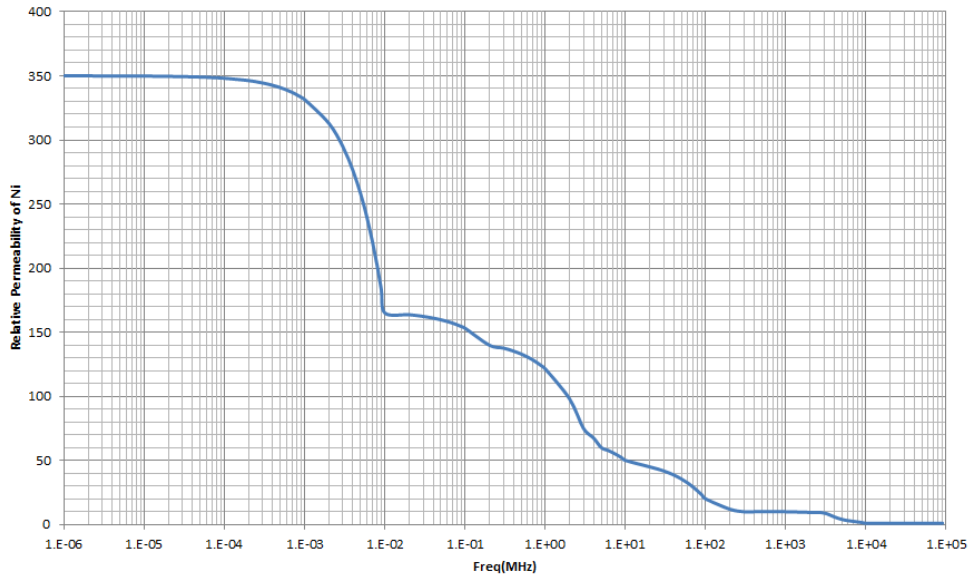


Figure 3-5 Ni relative permeability as a function of frequency

As a simple check of the plotted results in Figure 3-3, an independent calculation of the expected ac resistance of a solid copper wire can be performed using the relationship

$$r_{HF} = \frac{1}{2a} \sqrt{\frac{\mu_0}{\pi\sigma}} \sqrt{f} \quad \Omega/m \quad (78)$$

where  $a$  is the radius of the wire,  $\mu_0$  is the permeability of free space,  $\sigma$  is the conductivity of copper, and  $f$  is the operating frequency.

At 10 MHz, the curve in Figure 3-3 predicts an impedance value on the order of 350 milliohms per meter. For a 20 AWG solid copper wire, equation (78) predicts an impedance value of 323 milliohms per meter, a very close agreement.

In Figure 3-3, it is interesting to note the onset of skin effect, denoted by convergence of the real and imaginary parts of the impedance, for the four different materials. This occurs at a fairly low frequency for the nickel, between 3 kHz and 4 kHz. For the silver and copper materials, skin effect sets in almost two decades higher,



occurring between 100 kHz and 200 kHz. Finally, for the tin, the skin effect sets in between 1 MHz and 2 MHz. Clearly, for the solid wire case shown in Figure 3-3, the nickel wire exhibits a complex behavior driven by the permeability of the material. Note that above 10 GHz, the impedance of the nickel wire falls below that of the tin wire. Nickel is more conductive than tin, and above 10 GHz, the permeability of the nickel has dropped to the same as that of free space, so it is no longer dominating the behavior of the wire. The tin wire has a smoothly increasing behavior similar to the silver and copper wires, but is offset by the much lower conductivity of the material.

In Figure 3-4, the onset of skin effect for the three plated wires is quite different in the case of the nickel and tin platings as compared to that shown in Figure 3-3. The onset of skin effect for both the silver and tin plated wires is nearly coincident, showing a decrease factor of 10 for the tin, as compared to the virgin metal. In the case of the nickel plating, the onset is still lower in frequency as it was in Figure 3-3, but is much closer to that of the silver and tin wires, occurring between 30 kHz and 40 kHz, an increase factor of 10 as compared to the virgin metal. In Figure 3-4, while the behavior of the silver plated wire appears unchanged from that of the solid case, the behavior of the tin and nickel plated wires is markedly different. Now, the tin plated wire has an impedance curve that closely follows that of the silver plated wire up to about 7 MHz. At that frequency, the imaginary part of the impedance begins to deviate from the smoothly increasing trend, and this deviation continues to grow as the frequency increases. This behavior is expected as the skin effect becomes more dominant. With an increasing amount of current crowding to the outer periphery of the wire, and consequently becoming more concentrated in the tin plating layer, the impedance will increase until it is very nearly equal to that of the virgin tin metal. This behavior highlights why the use of tin plated wire for operations in and above the HF frequency range (3 MHz – 30 MHz) is not desirable.

The behavior exhibited by the tin plated wire in this analysis is echoed by results in Fowler's paper [38] in his Figure 6, wherein he clearly shows for a frequency of 10 MHz the relative resistivity of a 0.25 in diameter copper conductor plated with varying thicknesses of metals having unity permeability and varying conductivities steadily increasing in magnitude as a function of both plating thickness and material conductivity.

In contrast to the silver and tin plated wires, the nickel plated wire has a very interesting behavior, with the real and imaginary parts failing to converge at the onset of the skin effect near 40 kHz. The magnitude of the impedance remains above that of the tin or silver plated wires, running about 3 times as high above 1 MHz. Note also the real and imaginary parts exhibit multiple crossover points occurring near 10 MHz, 100 MHz, 300 MHz, and a final one near 4 GHz. The behavior exhibited by the nickel plated wire in this analysis is echoed by results in Fowler's paper [38] in his Figure 7, wherein he clearly shows for a frequency of 10 MHz the relative resistivity of a 0.25 in diameter copper conductor plated with varying thicknesses of nickel steadily increasing in magnitude as a function of both plating thickness and material permeability. This behavior also echoes that demonstrated by Graf [39], who shows the quality factor (Q) for a small coil of nickel plated copper wire is directly dependent on the thickness of the plating layer. Graf shows a set of curves that reflect a series of increasingly larger peaks in the coil Q as a function of both frequency and plating layer thickness, exhibiting the largest peak near 1 MHz for a 2  $\mu\text{m}$  thick plated layer. This thickness is comparable to the 50  $\mu\text{-in}$  plating thickness used in this work, and commonly found in the electrical, electronic, and aerospace industries. Note that Graf reports the permeability of the nickel plating on the wire sample in his experimentation is equal to 50. This determination appears to have been made at or near 10 MHz, which agrees very well with the predicted value shown in Figure 3-5 in this work. Finally, given the behavior shown in Figure 3-4, insertion loss behavior for

uniformly plated wires in a twisted shielded pair configuration would be expected to follow the impedance curves, with the tin plated wire exhibiting slightly greater loss than the silver plated wire as frequency is increased above a few MHz, and the nickel plated wire exhibiting loss greater than both the tin plated and the silver plated wires across the frequency range above a few hundred kHz.

As further exploration of the very interesting behavior of the Ni plating, three additional plots were produced using the numerical solution employed previously. In the first of these, in Figure 3-6, a comparison is shown of the behavior of “pure” Ni wire, “pure” Cu wire, and Cu wire plated with 50  $\mu\text{in}$  of Ni. This is entirely similar to Figure 3-4, with the exception of the addition of the “pure” Ni curve, illustrated in green colors. This set of curves has been discussed already and no further observations will be made here.

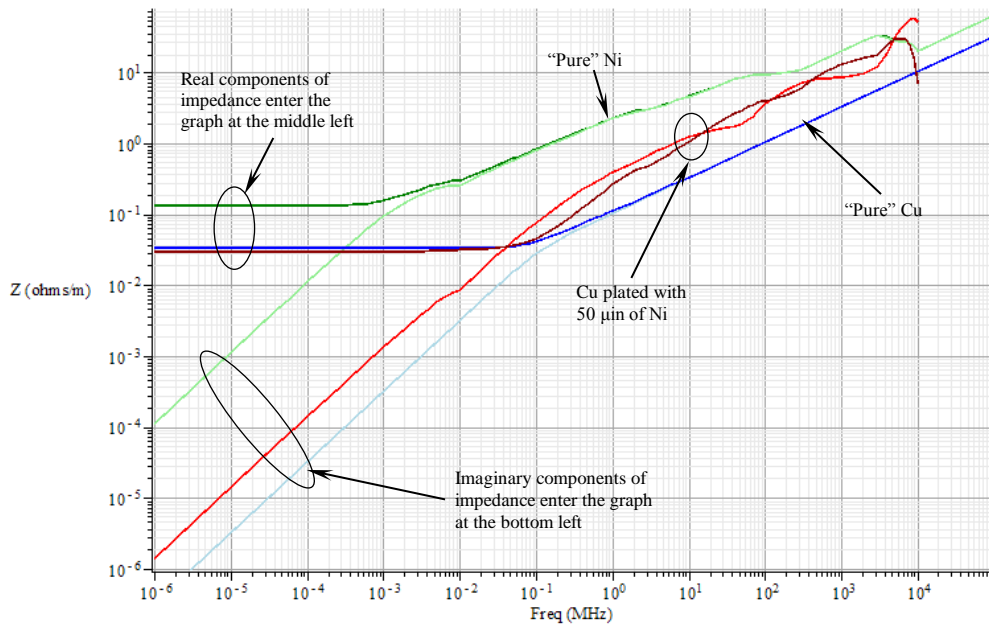


Figure 3-6 Comparison: “Pure” Ni vs “pure” Cu vs Cu plated with 50  $\mu\text{in}$  of Ni

In Figure 3-7, the Ni plating has now been increased to 161  $\mu\text{m}$ , very near to 10% of the radius of the 20 AWG wire examined here, a thickness described by Astbury [37], wherein he indicates

... a thin protective coating not exceeding some 10% of the total radius will have no significant effect on the electrical properties of the composite conductor. However, when the sheath thickness is of the same order as the core radius, ... the effective resistance of such a sheathed conductor might depend sharply on the current and might respond sharply to an ambient magnetic field. ...

Noticeable in Figure 3-7 is the lower dc resistance of the plated wire, the shift of the onset of skin effect to the left, the greater separation of the real and imaginary components of the plated wire between 100 kHz and 1 GHz, and the eventual convergence of the real and imaginary components near 1 GHz. Clear also in Figure 3-7 is the marked difference between the thinner and thicker coatings.

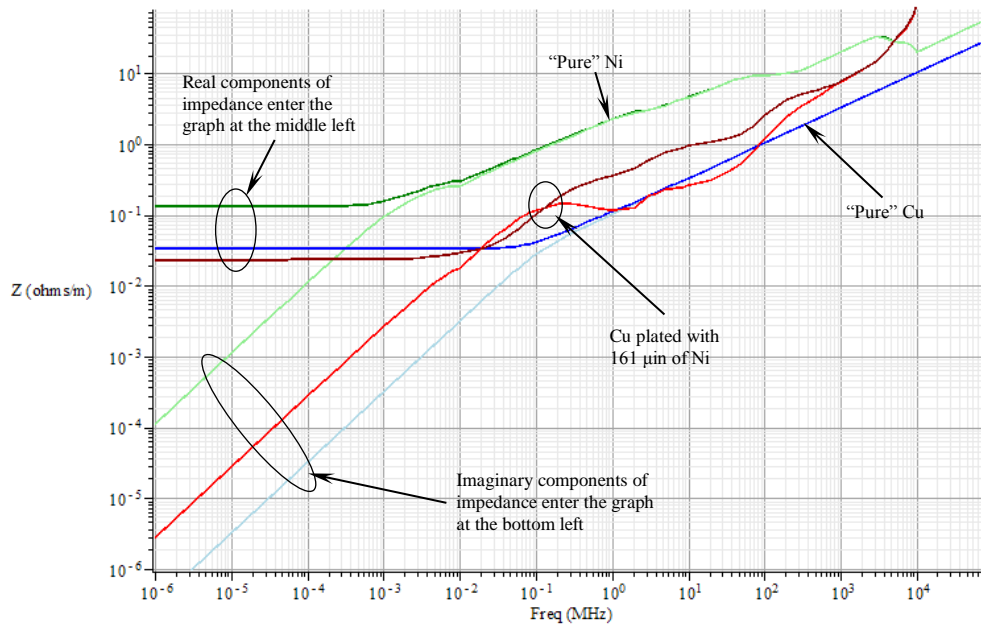


Figure 3-7 Comparison: "Pure" Ni vs "pure" Cu vs Cu plated with 161  $\mu\text{m}$  of Ni

Figure 3-8 illustrates the dramatic change from the previous coating thicknesses, specifically the much lower dc resistance, but also highlights the fact that even though the thickness of the coating is now a significant portion of the conductor radius, the behavior of the conductor is still not approaching that of the solid Ni conductor, except for the higher frequency range above 100 MHz. Another interesting aspect is the observation that skin effect onset is near to the same frequency of “pure” Cu, and the impedance of the Ni plated wire is actually lower than that of “pure” Cu below about 7 MHz.

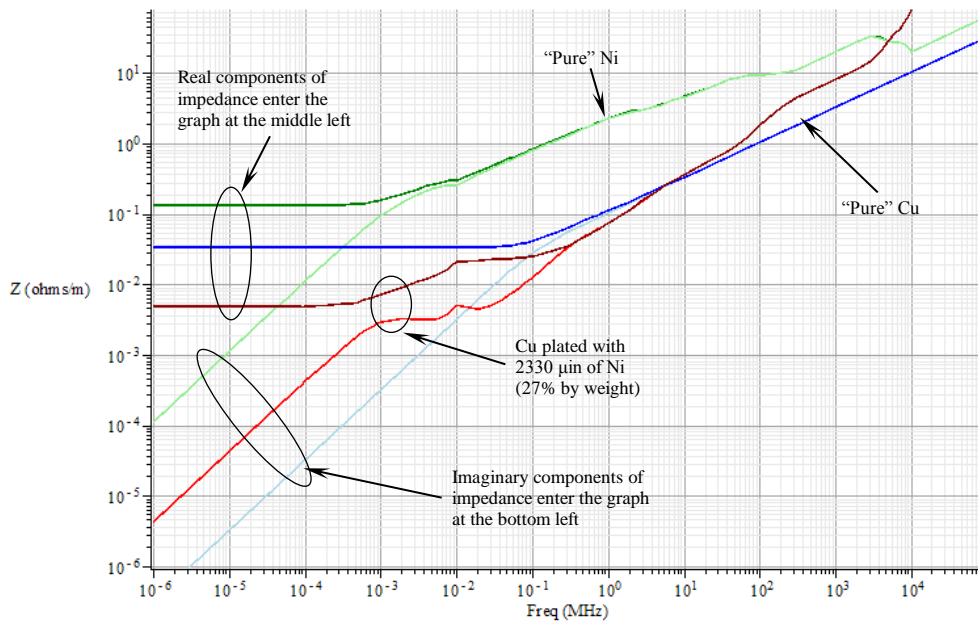


Figure 3-8 Comparison: “Pure” Ni vs “pure” Cu vs Cu plated with 2330  $\mu$ in of Ni

These last three Figures illustrate the wide variation of behavior associated with Ni plated Cu wire in a clear graphical sense, and strongly suggest potential for tailoring of the thickness of Ni plating on Cu wire may be realizable, depending on the application.

## Chapter 4

### Measurements

In order to validate the predicted results in Figure 3-4, a method was needed to measure the very small impedance of each type of plated wire. Since this work was intended to address “real world” applications, 2 meter samples of tin plated, silver plated, and nickel plated military specification wire as are commonly used in aerospace applications were obtained from a wire vendor. In particular, the samples were as follows:

- 1) M22759/32-20-9 – this is a 20 AWG stranded wire comprising 19 strands of 32 AWG tin plated copper conductors with a cross-linked, extruded, modified ethylene tetrafluoroethylene (ETFE) copolymer jacket, white in color
- 2) M22759/11-22-0 – this is a 22 AWG stranded wire comprising 19 strands of 34 AWG silver plated copper conductors with an extruded, polytetrafluoroethylene (TFE) polymer jacket, black in color
- 3) M22759/41-18-3 – this is an 18 AWG stranded wire comprising 19 strands of 30 AWG nickel plated copper conductors with a double layer of cross-linked, extruded, modified ethylene tetrafluoroethylene (ETFE) copolymer, orange in color
- 4) M27500-22SB2T23 – this is a twisted shielded pair of 22 AWG stranded wires, each comprising 19 strands of 34 AWG tin plated copper conductors with a cross-linked, extruded, modified ethylene tetrafluoroethylene (ETFE) copolymer jacket over each wire. The wires lay from 1 to 3 twists per inch. The twisted wires are covered with a braided shield comprising 38 AWG tin plated copper wires. The shielded pair is then covered by a cross-linked, extruded, modified ethylene tetrafluoroethylene (ETFE) copolymer jacket, white in color.

- 5) M27500-20SR2S23 – this is a twisted shielded pair of 20 AWG stranded wires, each comprising 19 strands of 32 AWG silver plated copper conductors with a cross-linked, extruded, modified ethylene tetrafluoroethylene (ETFE) copolymer jacket over each wire. The wires lay from 1 to 3 twists per inch. The twisted wires are covered with a braided shield comprising 38 AWG tin plated copper wires. The shielded pair is then covered by a cross-linked, extruded, modified ethylene tetrafluoroethylene (ETFE) copolymer jacket, white in color.
- 6) M27500-20SS2N23 – this is a twisted shielded pair of 20 AWG stranded wires, each comprising 19 strands of 32 AWG nickel plated copper conductors with a cross-linked, extruded, modified ethylene tetrafluoroethylene (ETFE) copolymer jacket over each wire. The wires lay from 1 to 3 twists per inch. The twisted wires are covered with a braided shield comprising 38 AWG tin plated copper wires. The shielded pair is then covered by a cross-linked, extruded, modified ethylene tetrafluoroethylene (ETFE) copolymer jacket, white in color.

Several different approaches were attempted to measure the impedance behavior of the single wire samples. Using the predicted curves, the range of expected resistance values for a six inch long wire sample would fall somewhere between 15 milliohms and 300 milliohms between frequencies from 1 MHz to 10 MHz for any of the three samples. The first attempt used a rather simple setup [63] employing a signal oscillator and an oscilloscope, as shown schematically in Figure 4-1. A standard laboratory RF signal generator was used to provide the applied voltage at the left of the circuit, and a standard 50 ohm splitter was used, together with a 50 ohm resistor for the known resistance R. Using the vector relationships amongst the various voltages in the

circuit, and the phase difference between the voltages measured at the two oscilloscope inputs, it is possible to determine the real and imaginary components of the unknown impedance, shown as  $Z$  in Figure 4-1. Unfortunately, as proved to be the case, this circuit did not exhibit sufficient dynamic range to complete the measurement of the expected very small resistance values, on the order of 15 milliohms, using the 50 ohm standard splitter and known resistance. Smaller values were attempted, but it soon became apparent that in order to resolve the expectedly very small unknown impedance, the values for the splitter and the known resistance would need to be near the value of the unknown itself, leading to noise floor issues with the output of the generator and resolution issues associated with the voltage differential between the oscilloscope inputs because of the very small voltages being measured, so this approach was abandoned.

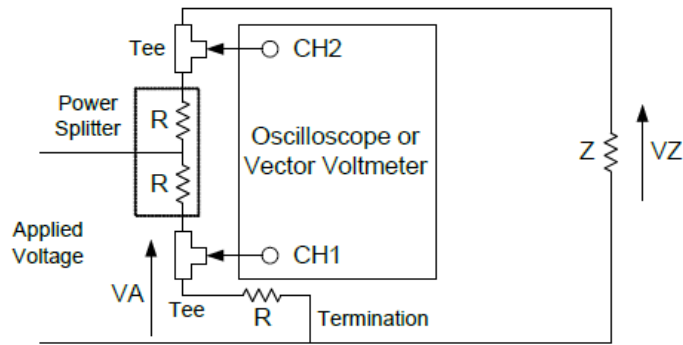


Figure 4-1 1<sup>st</sup> measurement attempt setup [63]

The next approach was to fabricate a small test fixture that could be used with a vector network analyzer (VNA) to collect the wire impedance data using a modified Kelvin 4 wire bridge configuration [64]. The fixture, made by Wetterlin and shown schematically in Figure 4-2, was very simple in configuration, comprising two 50 ohm resistors in series with each other and the VNA input/output (I/O) cables, with a 10 ohm resistor tied between the junction of the two 50 ohm resistors and the return side of the measurement



circuit. A wire sample would then be located in parallel with the 10 ohm resistor for the actual measurement. This fixture was constructed using a single-sided 1 ounce copper clad board, milled out to provide for the circuit paths and interconnections for the resistors and the wire sample.

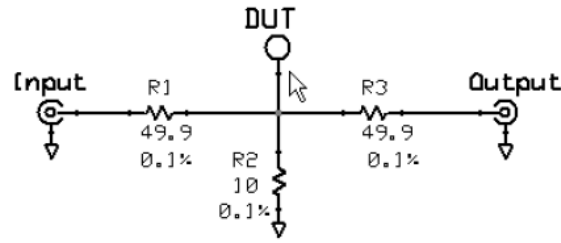


Figure 4-2 2<sup>nd</sup> measurement attempt fixture [64]

Two short lengths of RG-58 A/U cable were attached to the fixture to provide a convenient means of connecting the fixture to the VNA I/O cables. While this fixture was relatively simple in design and construction, and enabled some ease of attachment for the wire sample, it was extremely difficult to calibrate the VNA to shift the measurement planes to the wire sample under test, and after some few days spent on this configuration, like the first effort this too was abandoned.

After much searching and study, a solution appeared to present itself in the form of a fixture and methodology known as Thru-Reflect-Line (TRL). This is a process for calibration and measurement developed in the late 70's, and well documented in the literature. The recognized seminal paper on the topic [65] describes the method in some detail, and makes clear the process greatly simplifies the VNA calibration procedure. In brief, three "standards" are required, a "Thru", a "Reflect" (either an open or short), and a "Delay Line". The design constraints of such a set of standards are discussed in several references, but four in particular were extremely helpful [66-69]. The first of these provided excellent information with respect to the fundamental operation of the TRL

approach, then addressed error sources and types of measurements that could be made using TRL. Following this, design equations were provided for the various parameters and electrical characteristic of the standards, with guidance on their application and determination. The next two references from Agilent provided excellent detail on the physical and electrical dimensions of the components of a set of TRL standards, thereby greatly facilitating the design process. The fourth reference was not specifically related to the use of TRL fixtures, but directly addressed the measurement of very small impedances, and provided additional guidance and constraint on both physical and electrical dimensions for the set of TRL standards. This reference also provided excellent guidance and information with respect to the 4 wire Kelvin measurement approach, wherein the device under test is connected in parallel across the measurement plane. The VNA is then connected and S21 data is collected, providing much better resolution for very small impedance values than is possible with a more traditional S11 reflection measurement.

Armed with the above information, a set of standards was designed in microstrip format on a double layer 1 ounce copper board having an FR4 substrate. The Thru and Line were designed to exhibit a 50 ohm characteristic impedance, and an open was chosen for the Reflect, being easier to construct than a short. The three standards were fabricated using a nominal etching process. The Thru was designed with a 1 inch length extending from one side of the strip to accommodate the attachment of the wire samples. A photograph of the design sketches showing the dimensions of the standards is shown in Figure 4-3. The standards themselves are also in the photograph, laid on or adjacent to the corresponding sketch. Close-ups of the three standards are provided in Figures 4-4 through 4-6. Note that the Thru has a wire sample in place, ready for measurement.

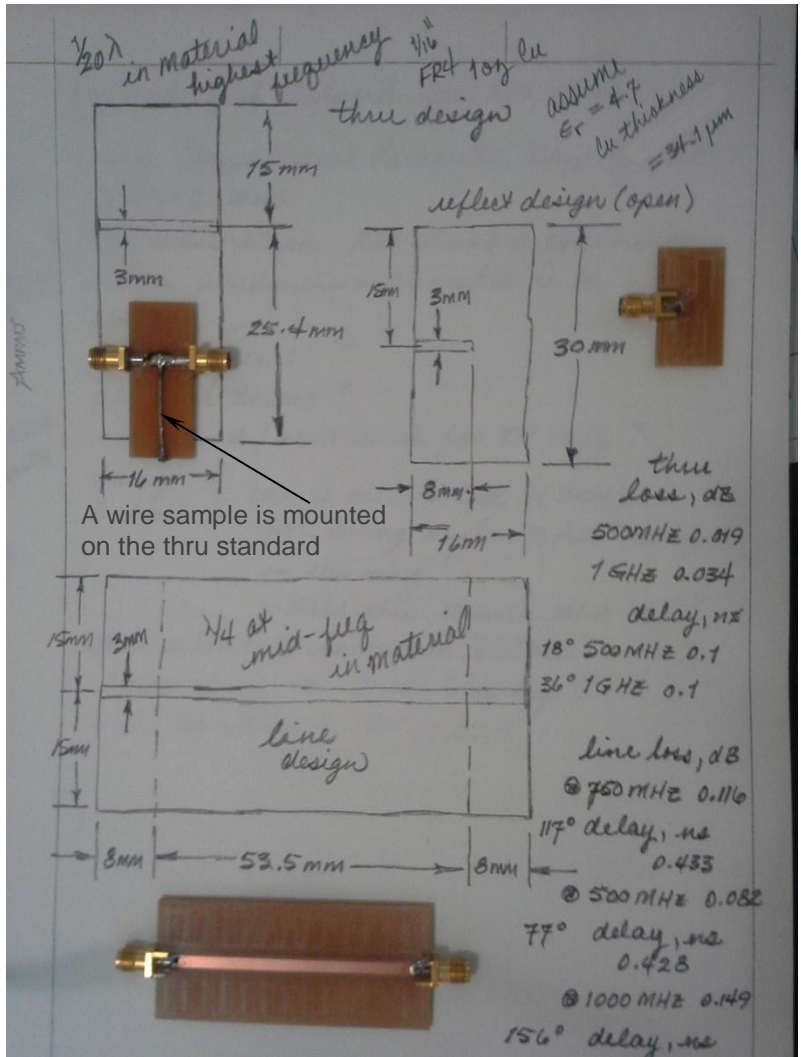


Figure 4-3 TRL standards on design sketches

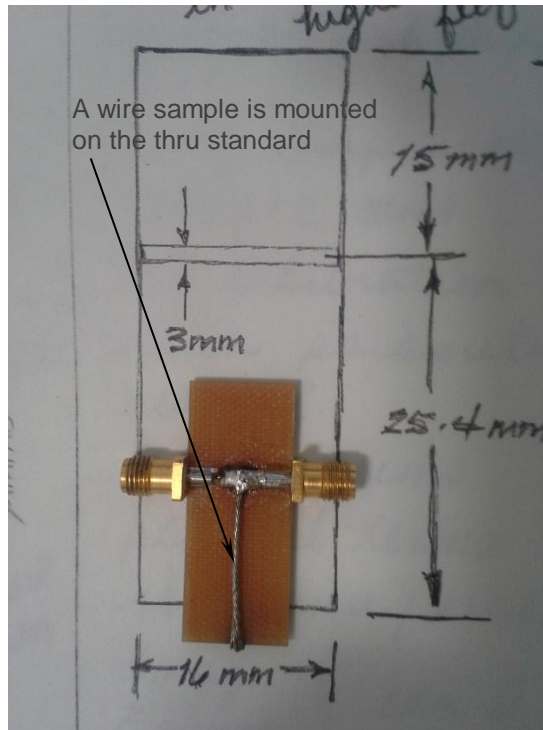


Figure 4-4 Thru TRL standard

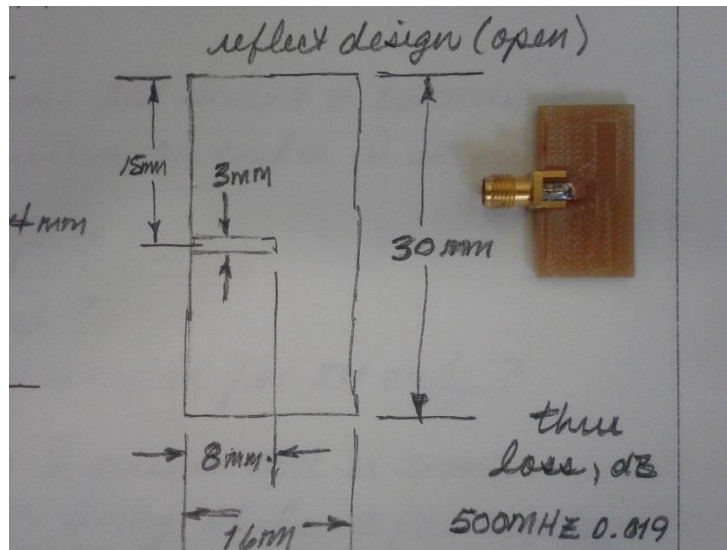


Figure 4-5 Open TRL standard

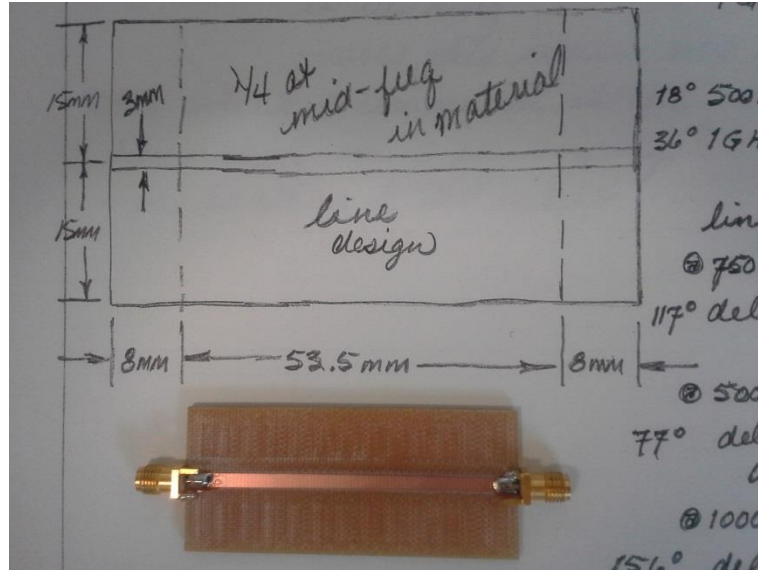


Figure 4-6 Line TRL standard

Once the set of standards was completed, the VNA was programmed with the calibration fixture characteristics, and calibration proceeded in accordance with Agilent's direction [70]. After calibration, individual wire samples were carefully soldered into place across the 1 inch length of the Thru standard. The measured data were very skewed, indicating the presence of a large amount of parasitic inductance. After some thought, it became apparent that the inductance of the wire sample above the ground plane of the Thru standard was directly affecting the measurement accuracy. In an effort to identify, and possibly extract this parasitic inductance, its value, 9.5 nH, was estimated using the relationship

$$l = \frac{\mu_0}{2\pi} \ln \left( \frac{h}{r} + \sqrt{\left(\frac{h}{r}\right)^2 - 1} \right) H/m \quad (78)$$

where  $h$  is the height of the wire above the ground plane, measured from the surface of the ground plane to the center of the wire, and  $r$  is the radius of the wire.

At 10 MHz, this value of inductance would contribute some 593 milliohms to the measured data. At 100 MHz, this value would increase to approximately 6 ohms, significantly greater than the expected maximum of 300 milliohms. At this point, a consultation was opened with Agilent Technical Support. After several more days of working with the Agilent representative, it was decided that measurement of the single wire sample using the TRL fixture would not produce any accurate results.

As a means of moving forward, a new version of the Wetterlin fixture was designed and built. This version, shown in Figure 4-7, was made as small as possible, using series 0603 and 0402 surface mount components.

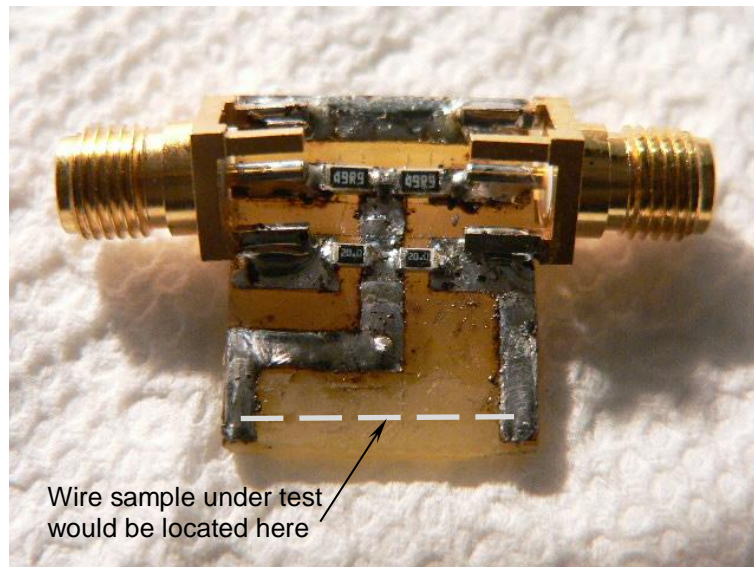


Figure 4-7 Improved Wetterlin fixture

The series 0603 49.9 ohm resistors can be seen at the top of the fixture, directly in line with the center pins of the two SMA connectors. The 10 ohm resistor was split into two series 0402 20.0 ohm resistors in parallel. These can be seen below the 49.9 ohm resistors, in line with the lower frame leg of the two SMA connectors. Measurements

proceeded with a very careful full two-port calibration of the VNA, using an IF bandwidth of 1 kHz, averaging set to 16, and a frequency range from 1 MHz to 100 MHz. On this fixture, the wire samples were only ½ inch in length, so the data was expected to be quite small in magnitude. Figure 4-8 shows representative data captured using this fixture.

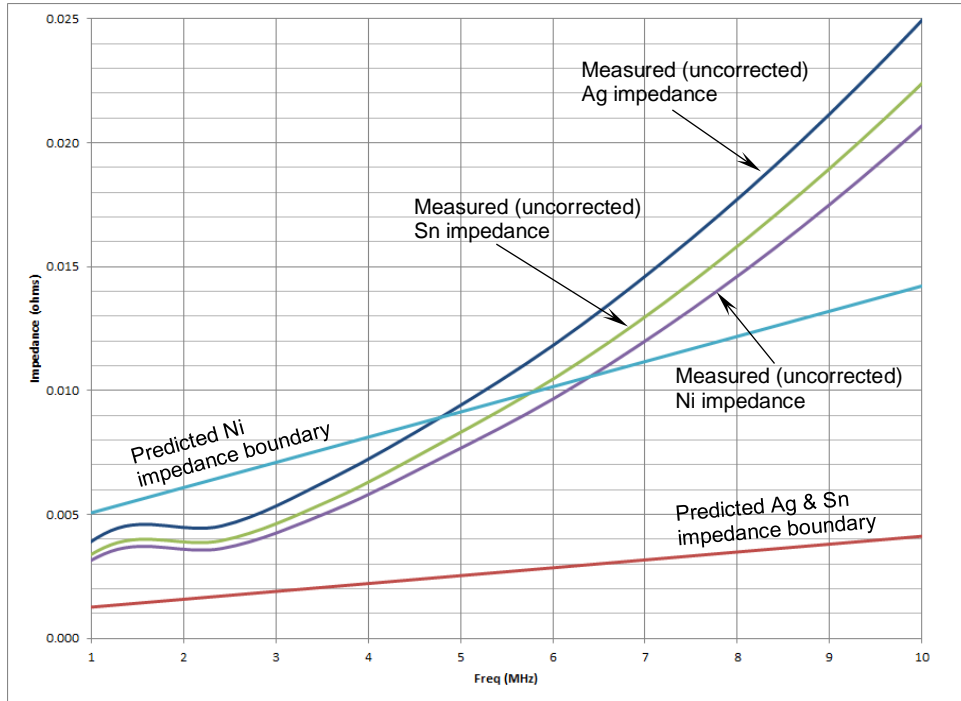


Figure 4-8 Data captured using the improved Wetterlin fixture

Examination of this plot shows that the data collected is still affected by some large parasitic inductance somehow not accounted for in the calibration of the VNA or in the intervening structure of the fixture itself. Also, the data appears to be inverted, in that the nickel sample is exhibiting lower impedance than either the tin or silver plated wire samples. However, it is apparent that this improved fixture is able to resolve the smaller impedance values at the low end of the frequency range, up to near 5 MHz, although the accuracy still leaves much to be desired.

Physical examination of the fixture suggested that a mutual inductance presented by the short, parallel lengths of copper strip visible at the bottom on either side of the Improved Wetterlin fixture may have played a role in the error. Estimating the length of the parallel strips to be 0.325 cm, and their separation to be 1.4 cm, and using the relationship [71], the mutual inductance was found as follows:

$$M = \frac{\mu_0}{2\pi} \left( l \sinh^{-1} \frac{l}{d} - \sqrt{l^2 + d^2} + d \right) H = 150.23 \text{ pH} \quad (79)$$

where  $l$  is the common length of the two strips and  $d$  is their separation.

Extracting this value of inductance from the raw data, and assuming a slight increase in the magnitude as a function of frequency commensurate with the increase of the ac resistance of the wire sample under test, enabled a very satisfactory correction to the data as shown in Figure 4-9.

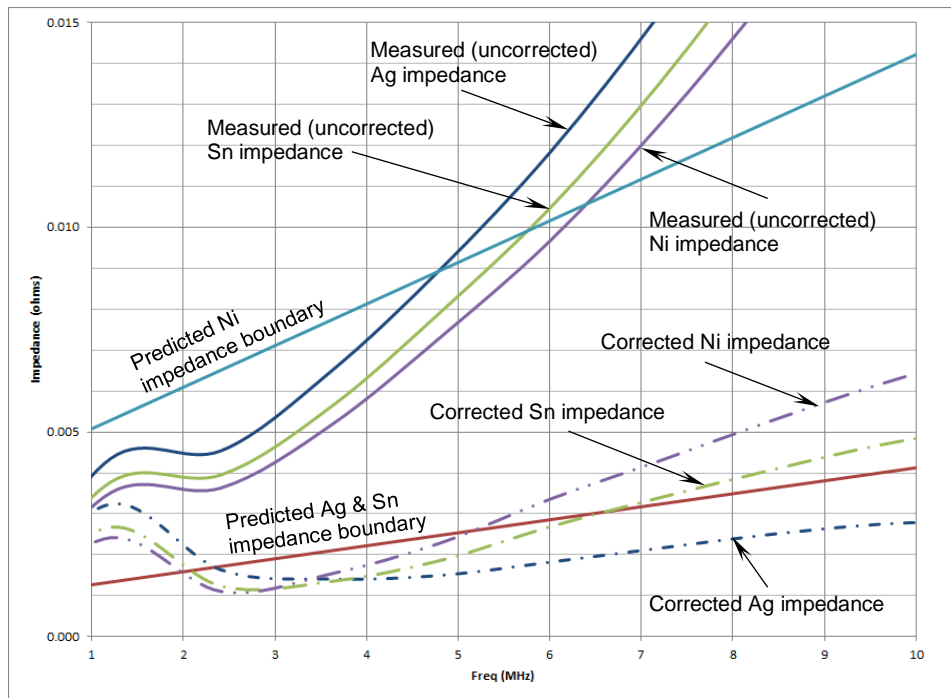


Figure 4-9 Corrected data using the improved Wetterlin fixture



As can now be observed, the behavior of the three plated wires is much closer to the predicted boundaries, with the Ag plated wire running just beneath and nearly parallel to the predicted bounding limit, the Sn plated wire crossing near 7 MHz, in agreement with the earlier predicted split of the real and imaginary components while still falling between the Ag and the Ni plated wires, and the Ni plated wire crossing and then running in near parallel to the predicted limit.

The next step was to try a new and completely different approach to the collection of data to illustrate the behavior of the plated wire samples. It was determined the best way to proceed was to measure the insertion loss of the twisted shielded pair samples as a function of frequency. The characteristic impedance of the samples was checked by measuring the impedance of each of the two meter samples, first with the conductors shorted together, and then with the conductors open. Using the well-known relationship

$$Z_0 = \sqrt{Z_s \times Z_o} \quad (80)$$

and the complex impedance data collected for each sample, the characteristic impedance for each of the twisted shielded wire samples was found to be:

- 1)  $Z_{Sn} = 112.6 \Omega$
- 2)  $Z_{Ni} = 107.4 \Omega$
- 3)  $Z_{Ag} = 100.4 \Omega$

Two North Hills 50 ohm to 124 ohm baluns [72,73] were located for use in the insertion loss measurement setup with the VNA. No baluns were available with a value closer to the characteristic impedance of the wire samples, but it was decided to move on, since the mismatch would be small in all three cases, and the data was meant to be relative for comparison, and not absolute. Figure 4-10 shows the general setup, a close-

up of the wire sample connected between the two baluns is shown in Figure 4-11, and Figure 4-12 shows a close-up of one of the baluns nomenclature plate.

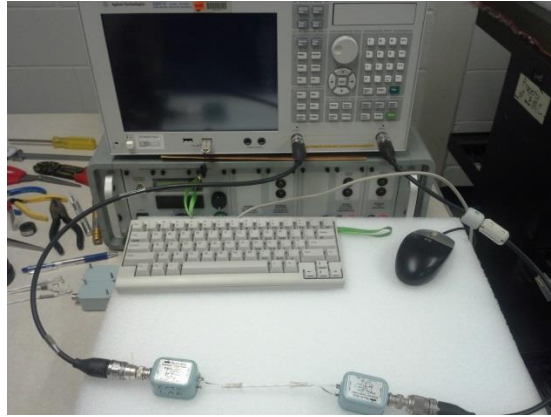


Figure 4-10 General insertion loss setup

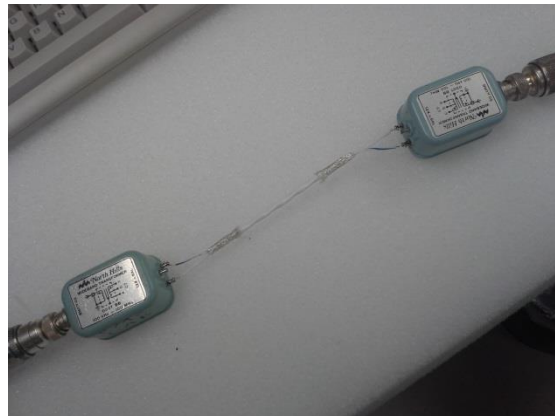


Figure 4-11 Close-up of wire connected to baluns



Figure 4-12 Close-up of balun nomenclature plate

A six inch long section was cut from each of the three twisted shielded pair samples and measured for insertion loss from 1 MHz to 100 MHz. Based on the data shown in Figure 3-4, the nickel plated wire sample was expected to exhibit a higher insertion loss across this entire frequency range, with the tin and silver plated wire samples behavior more closely coincident. Note the use of the ferrite beads on the port 2 cable to the VNA. This was found to be of great benefit in the data collection, since without these beads, the data had several unexplained maxima across the frequency range. A bit of research into this effect uncovered information from Agilent concerning how common mode noise might impact VNA measurements. A diagram from one of the references [74], shown in Figure 4-13, depicts the issue, and shows the use of ferrite beads or common mode chokes to defeat the effect.

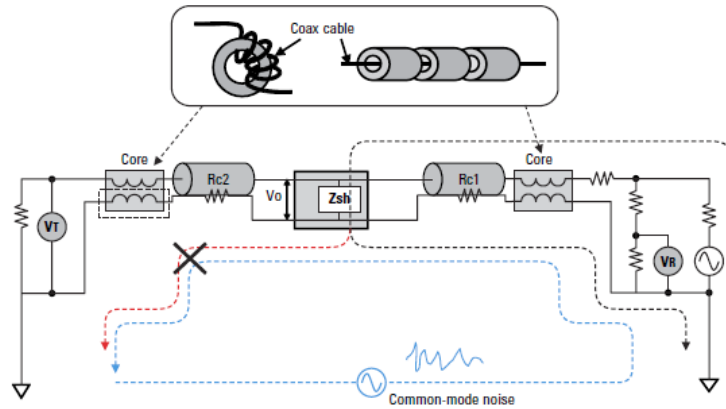


Figure 4-13 Suppression of common mode noise in VNA measurement [74]

This same technique is briefly discussed in a paper addressing the measurement of very small impedances of power distribution networks [75]. In the insertion loss measurement setup for the twisted shielded pairs, baluns were used so currents directly common between the ports would be unexpected. But there were clearly still parasitic currents flowing on the cable shield to port two since the use of the beads completely suppressed this effect. The most likely cause was radiated emissions from the wire samples under test coupling onto the current loop from port 2 through the balun winding, and back to the port, as can be surmised from the right hand side of Figure 4-13. Considering the small voltages being measured, only a small amount of current would be necessary to introduce interference into the measurement.

S21 data was collected for each sample, and is shown in Figure 4-14. This data clearly shows the expected trend in the insertion loss behavior of the three plated wire samples.

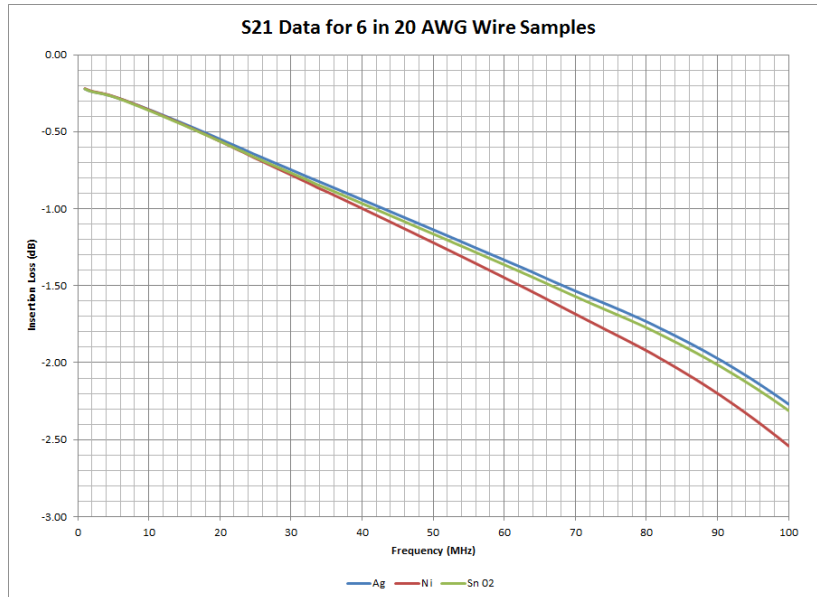


Figure 4-14 S21 data for twisted shielded wire pairs

The tin and silver plated samples are nearly coincident, with the tin plated sample loss exhibiting a slight tendency to increase as frequency increases, whereas the nickel plated sample is below the other two samples, and is continuing to show an increasing loss across the entire frequency range. Extrapolation to the same frequency range, 1 MHz to 100 MHz, of data collected by an independent group in 2000 [76] for cable attenuation of 30 AWG and 28 AWG twisted unshielded wiring showed similar behavior, lending credence to the accuracy of the data collected in this work.

Before leaving this chapter, it should be noted that the measurement of the impedance of plated wire samples is exceedingly difficult, as evidenced by the many attempts to do so documented in this work. A robust and accurate method remains to be developed as future work.

## Chapter 5

### Discussion

A comparison of the behaviors shown in Figures 3-3 and 3-4 reveals some of the key findings of this work. Figure 3-3 illustrates the behavior of four different materials commonly used in electrical work. In this Figure, it is interesting to note the onset of skin effect, denoted by convergence of the real and imaginary parts of the impedance, for the four different materials. This occurs at a fairly low frequency for the nickel, between 3 kHz and 4 kHz. For the silver and copper materials, skin effect sets in almost two decades higher, occurring between 100 kHz and 200 kHz. For the tin, the skin effect sets in between 1 MHz and 2 MHz. The tin wire has a smoothly increasing behavior similar to the silver and copper wires, but is offset by the much lower conductivity of the material. Finally, it is interesting to note the behavior of the pure silver wire, between 1.05 and 1.08 times as conductive as copper, is nearly coincident with that of the pure copper wire across the entire frequency range.

Most importantly, for the solid wire case shown in Figure 3-3, the nickel wire exhibits a complex behavior driven by the permeability of the material. Note that above 10 GHz, the impedance of the nickel wire falls below that of the tin wire. Nickel is more conductive than tin, and above 10 GHz, the permeability of the nickel has dropped to the same as that of free space, so it is no longer dominating the behavior of the wire. This complex behavior will manifest itself again in the case of a nickel plated copper cored wire, as can be observed in Figure 3-4.

In that Figure, the onset of skin effect for the three plated wires is quite different for the nickel and tin platings as compared to that shown in Figure 3-3. The onset of skin effect for both the silver and tin plated wires is now nearly coincident, showing a decrease factor of 10 for the tin, as compared to the virgin metal. In the case of the nickel

plating, the onset is still lower in frequency as it was in Figure 3-3, but is much closer to that of the silver and tin wires, occurring between 30 kHz and 40 kHz. This is an increase factor of 10 as compared to the virgin metal.

Note also the behavior of the plated wires as a function of frequency. The silver plated wire appears unchanged from that of the solid case. Notably, this behavior also remains nearly coincident with that of the pure copper wire shown in Figure 3-3. The behavior of the tin and nickel plated wires is markedly different from that shown for these materials in Figure 3-3. Now, the tin plated wire has an impedance curve that closely follows that of the silver plated wire up to about 7 MHz. At that frequency, the imaginary part of the impedance begins to deviate from the smoothly increasing trend, and this deviation continues to grow as the frequency increases. This behavior is expected as the skin effect becomes more dominant. With an increasing amount of current crowding to the outer periphery of the wire, and consequently becoming more concentrated in the tin plating layer, the impedance will increase until it is very nearly equal to that of the virgin tin metal. This behavior highlights why the use of tin plated wire for operations in and above the HF frequency range (3 MHz – 30 MHz) is not desirable.

The behavior exhibited by the tin plated wire in this analysis is echoed by results in Fowler's paper [38], shown in Figure 5-1, wherein he clearly shows for a frequency of 10 MHz the relative resistivity of a 0.25 in diameter copper conductor plated with varying thicknesses of metals having unity permeability and varying conductivities steadily increasing in magnitude as a function of both plating thickness and material conductivity.

As expected in contrast to the silver and tin plated wires, the nickel plated wire has a very interesting and complex behavior shown in Figure 3-4, with the real and imaginary parts failing to converge at the onset of the skin effect near 40 kHz.

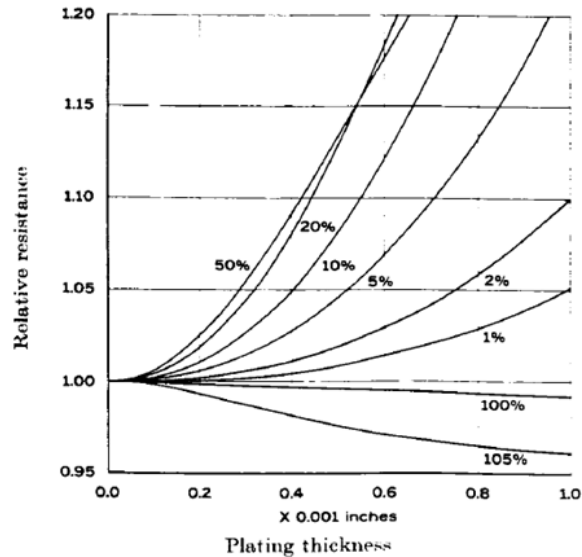


Figure 6.—A.C. resistance, at 10 MHz, of a 0.25 in dia. copper rod (conductivity 100% I.A.C.S.) plated with metals of various conductivities, and unity permeability (enlarged section of fig. 5).

Figure 5-1 Figure 6 from Fowler [38]

The magnitude of the impedance remains above that of the tin or silver plated wires, running about 3 times as high above 1 MHz. Note also the real and imaginary parts exhibit multiple crossover points occurring near 10 MHz, 100 MHz, 300 MHz, and a final one near 4 GHz.

The behavior exhibited by the nickel plated wire in this analysis is again echoed by results in Fowler's paper [38], shown in Figure 5-2, wherein he clearly shows for a frequency of 10 MHz the relative resistivity of a 0.25 in diameter copper conductor plated with varying thicknesses of nickel steadily increasing in magnitude as a function of both plating thickness and material permeability.

This behavior also echoes that demonstrated by Graf [39], who shows the quality factor (Q) for a small coil of nickel plated copper wire is directly dependent on the thickness of the plating layer. Graf shows a set of curves, shown in Figure 5-3, that reflect



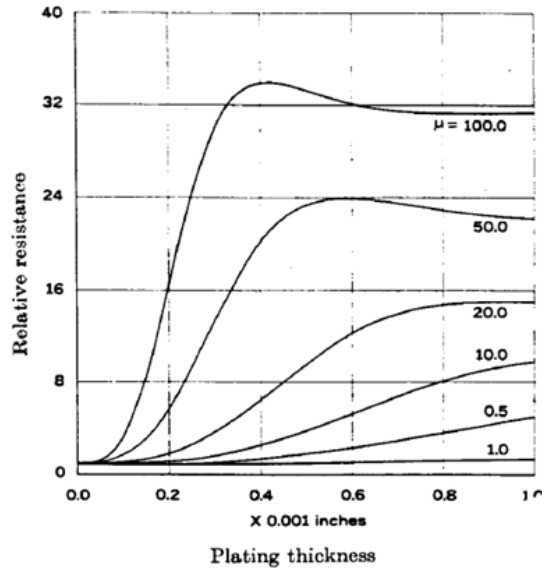


Figure 7.—A.C. resistance, at 10 MHz, of a 0.25 in dia. copper rod (100% I.A.C.S.) plated with metals of various permeabilities, and a conductivity of 10% I.A.C.S.

Figure 5-2 Figure 7 from Fowler [38]

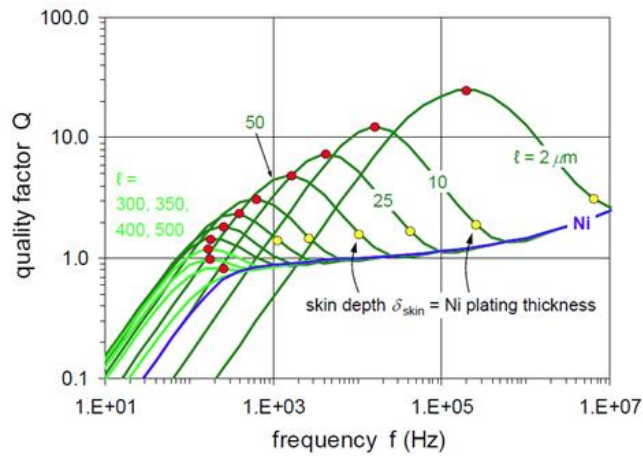


Figure 5-3 Figure by Graf [39]

a series of increasingly larger peaks in the coil Q as a function of both frequency and plating layer thickness, exhibiting the largest peak near 2 MHz for a 2 μm thick plated layer. This thickness is comparable to the 50 μ-in plating thickness used in this work, and commonly found in use by the electrical, electronic, and aerospace industries. Note that

Graf reports the relative permeability of the nickel plating on the wire sample in his experimentation is equal to 50. This determination appears to have been made at or near 10 MHz, which agrees very well with the predicted value shown in Figure 3-5 in this work.

Given the behavior shown in Figure 3-4, insertion loss behavior for uniformly plated wires in a twisted shielded pair configuration would be expected to follow the impedance curves, with the tin plated wire exhibiting slightly greater loss than the silver plated wire as frequency is increased above a few MHz, and the nickel plated wire exhibiting loss greater than both the tin plated and the silver plated wires across the frequency range above a few hundred kHz. This is borne out by the insertion loss measurements performed and documented in the latter portion of the preceding chapter, shown in Figure 4-13. The tin and silver plated samples are nearly coincident, with the tin plated sample loss exhibiting a slight tendency to increase as frequency increases, whereas the nickel plated sample is below the other two samples, and is continuing to show an increasing loss across the entire frequency range. Extrapolation to the same frequency range, 1 MHz to 100 MHz, of data collected by an independent group in 2000 [76] for cable attenuation of 30 AWG and 28 AWG twisted unshielded wiring showed similar behavior, lending credence to the accuracy of the data collected in this work.

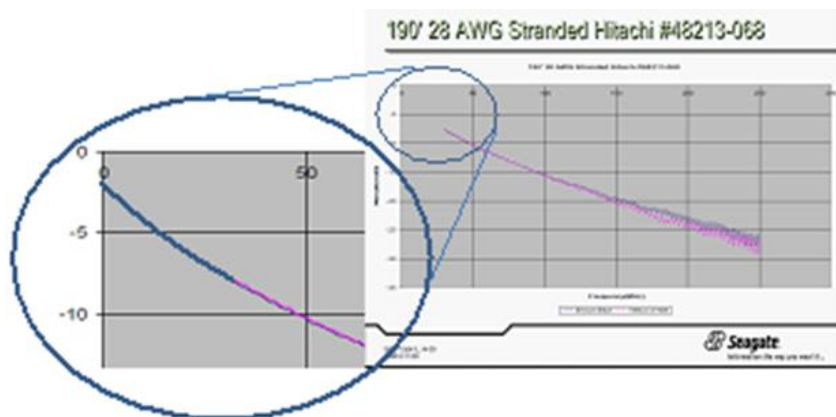


Figure 5-4 SCSI PIP Committee presentation [75]

These findings lead to some pragmatic results and applications that have the potential to reduce cost and mass impacts particularly in the aerospace and automotive industries. First of all, the use of a silver plating simply to extend the use of wiring to higher frequency ranges may not be warranted unless the application is for an extended service elevated operating temperature environment. This is well illustrated in Figures 3-3 and 3-4, wherein the behavior as a function of frequency of a pure copper conductor and that of a pure copper conductor plated with pure silver are nearly indistinguishable across a very wide frequency range extending well into the gigahertz region. This becomes even more interesting considering that the difference in conductivity of pure copper versus pure silver is not extreme, and the wire industry does not employ pure forms of either metal. Indeed, the governing ASTM standard [4] for silver plated wire requires the dc conductivity of the plated wire to be equivalent to that of a copper conductor formed from standard annealed copper, which itself exhibits a slightly lower conductivity than the pure metal. Silver used in plating copper wire contains a number of constituent components that aid in the plating process or enhance the appearance of the plated surface, but at the same time act to reduce the plating layer's conductivity, so that it may well be more effective from both a cost and efficiency perspective to simply plate an annealed copper conductor exhibiting a 100 % conductivity per the International Annealed Copper Standard (IACS) with a thin layer of very high conductivity copper, such as Oxygen Free Electronic (OFE) copper, Oxygen Free (OF) copper, or Electrolytic Tough Pitch (ETP) copper, all of which meet or exceed 101 % conductivity per the IACS, and then coat the outer layer with perhaps a high temperature clear lacquer finish to prevent the formation of copper oxides. Offering the same or possibly better performance across frequency while avoiding the cost of silver plating could present a dramatic decrease in

manufacturing and acquisition cost in applications where the higher temperature capability of a silver plated wire is not an overarching design consideration.

In the case of a tin plated wire, elevated temperatures accelerate the growth of the intermetallic layer that forms between the tin and copper, eventually reaching completion when the intermetallic layer has completely consumed the tin plating. This reduces the wire's solderability and can increase the resistivity of a crimped joint significantly. The process of intermetallic growth is independent of external influences such as the presence of moisture. Thus, this process cannot be stopped or slowed by attempting to seal a crimped joint. When compared to a tin plated wire, a silver plated wire clearly exhibits both superior long term service and superior elevated temperature performance.

In contrast, the surface of a non-plated copper wire exposed to the air, and depending on the temperature of the environment, will immediately form an external layer of either cuprous oxide or a combination of cuprous and cupric oxides. Both of these oxides are semi-conductive, and are much more resistive than the copper substrate. Cuprous oxide is the less conductive of the two, and forms at temperatures below 200° centigrade. The formation of these oxides is driven by elevated temperatures, and like intermetallic growth in a tin plated wire, is a function of time, and once the process starts, will continue to erode the surface of the copper substrate. Unlike the tin plated wire, however, if desired the formation of these oxides can be prevented by coating the outer layer of a composite copper conductor as described previously. The onset of oxide formation can also be controlled by sealing crimped joints to prevent the intrusion of air and moisture. The presence of copper oxides can act to reduce solderability in older copper conductors, but the oxides are in general easily removed by light abrasion preparatory to soldering operations. Here again the apparent advantage, and cost, of a

silver plated wire may be offset by proper and careful engineering design and application of a copper plated copper wire.

A second, and much more interesting, area of application is that involving the use of nickel plating on a copper conductor. Nickel is less expensive than silver, and offers a more extended operating temperature range. It does exhibit solderability difficulties, but these can be easily overcome through the use of appropriate solder fluxes and procedures for post-soldering cleansing. Of course, as with silver plating, annealed copper conductors with a plating layer of higher conductivity copper could be used to offset the solderability concerns for applications wherein the higher temperature range capability of nickel is not warranted. But the use of nickel plating offers a unique advantage in that it introduces the ability to incorporate high frequency attenuation characteristics directly into interconnecting wiring harness at a fraction of the cost and mass impact of adding low pass filter components or filter connectors. That this is the case can readily be understood by again examining the curves shown in Figures 3-3 and 3-4. Clearly as a function of frequency, a nickel plated conductor exhibits measurably higher impedance than does either a tin plated or silver plated conductor. Similarly, in Figure 4-13, a twisted shielded pair comprising nickel plated conductors enclosed by a nickel plated braided shield exhibits an insertion loss that is clearly increasing at a greater rate than either a tin plated or silver plated twisted shielded pair.

Even in cases where additional low pass filter components may still be required, the use of nickel plated wire can act to distribute filtering effects, requiring smaller, less expensive filter components at the terminations of the wiring harness. Incorporating nickel plated wire into the braided shield of a twisted shielded pair can add further immunity to signal and power lines, since any high frequency currents that might be induced to flow on the shielding will be attenuated in like fashion. This filtering action is in

direct proportion to the length of the wiring harness, and is extremely important in transient protection, wherein impulsive noise exhibiting fast rising and falling edges can be controlled by the distributed filtering action of nickel plated conductors.

Related work [77-81] from between 45 and 65 years ago, and apparently not pursued more recently, demonstrated that wire of any sort exhibits a transient response behavior quite similar to thermal diffusion, based on the distribution of current in the conductor. This work showed specifically that whenever a transient current enters a conductor, and in particular short, fast transients, the current distribution is primarily concentrated at or near the surface of the conductor, a natural expectation given the physics of skin effect. It is an easy step to surmise that, as the work documented herein shows, a nickel plating on a copper conductor substrate can play a direct and significant role in controlling this sort of interference.

## Chapter 6

### Highlights and Concluding Remarks

In summary, this work has explored the various aspects of platings on wire, focusing specifically on tin, silver, and nickel platings on copper conductors as used primarily in aerospace, and secondarily in a broader range of applications.

A detailed mathematical analysis and numerical code was developed to enable the calculation and prediction of the behavior of platings on conductors. Use of this analytical tool clearly showed a complex impedance behavior as a function of frequency for a nickel plated copper conductor, as compared to that of either a tin or silver plated copper conductor. The complexity of this behavior was found to be proportional to the thickness of the coating. This same analytical tool also showed the impedance behavior of a tin plated copper conductor follows that of a silver plated copper conductor or a pure copper conductor up to about 7 MHz, at which point the impedance begins to asymptotically approach that of a pure tin conductor. This behavior, like that of a nickel plated copper conductor, is directly affected by the thickness of the plating layer, exhibiting a more rapid deviation towards that of a pure tin conductor as the thickness increases.

The relative permeability curve for nickel shown in Figure 3-5 is not known to exist elsewhere in the literature, and was developed from a compilation of multiple research sources. This curve was critical to the analysis and prediction of the impedance behavior of a nickel plated copper conductor.

This work shows that a strong potential exists for significant cost savings to be realized from the use of high conductivity oxygen free or electrolytic tough pitch copper as a plating layer for standard 100% IACS copper conductor, instead of more expensive

silver plating, where silver's elevated temperature performance is not a design consideration.

Most importantly, this work has shown a number of measurement methods, many of which proved not to be useful for the measurement of the very small impedance changes associated with wire plated with differing metals. Even so, a successful measurement method is shown, together with the necessary extraction of fixture parasitics.

This research opens the door to much additional work that can benefit engineering activity associated with the use of wired systems in aerospace, automotive, and other electrical and electronic industries. Effort must be combined with an educational program to begin enlightening engineers and platers alike to the needs of the electrical, electronic, and aerospace industries in the careful and meticulous design of plated wires for applications in RF circuitry, and more importantly for protection from high frequency interference and high speed transients. A more robust and reliable means of measuring the magnetic behavior of nickel plated wires must be developed, together with research into the effects of plating thickness, and the patterning of thick and thin plating layers, on copper conductors. To this end, discussions have already been started with representatives from the National Institute of Standards and Technology (NIST) to explore the nuances and difficulties associated with the measurement setup. The specific transient response behavior of plated wires should be fully investigated, thereby laying the groundwork to accomplish the development of standards and specifications encompassing the appropriate requirements and design constraints for the employment of plated wires, in particular nickel plated wire.



## Appendix A

MAPLE Code for Numerical Computation of the Impedance of Plated Wire

```

# MAPLE Routine for Computation of Impedance of Plated Cylindrical Conductors
# Revision -
# Robert C. Scully
# October 2013
#
# Start Program
#
# Initialization routines
#
restart;
with(LinearAlgebra) : with(plots) : Digits := 20 :
#
# Definition of basic constants
#
mu0 := 4·evalf(Pi)·10-7 : c := 300·106 : e0 := (mu0·c2)-1 :

mu := Matrix(99, 3, fill = mu0) :
muNi := Vector[column]([350, 349.98, 349.96, 349.94, 349.93, 349.91, 349.89, 349.87, 349.85, 349.83,
349.65, 349.46, 349.28, 349.09, 348.91, 348.72, 348.54, 348.35, 348.17, 346.32, 344.47, 342.62,
340.77, 338.92, 337.07, 335.22, 333.37, 331.52, 313.02, 294.52, 276.02, 257.52, 239.02, 220.52,
202.02, 183.52, 165.0, 163.68, 162.37, 161.05, 159.74, 158.42, 157.10, 155.79, 154.47, 153.16,
140.00, 137.68, 135.36, 133.04, 130.72, 128.40, 126.07, 123.75, 121.43, 98.22, 75.00, 67.50, 60.00,
58.00, 56.00, 54.00, 52.00, 50.00, 45.00, 41.83, 38.67, 35.50, 32.33, 29.17, 26.00, 23.00, 20.00,
12.00, 10.00, 10.00, 10.00, 10.00, 10.00, 10.00, 10.00, 10.00, 10.00, 9.50, 9.00, 6.00, 4.00, 3.00, 2.50,
2.00, 1.50, 1.00, 1.00, 1.00, 1.00, 1.00, 1.00, 1.00, 1.00, 1.00]) :
mu := ((mu)(mu0·muNi)) :

eCu := 1·e0 : eAg := 1·e0 : eSn := 1·e0 : eNi := 1·e0 :
e := Vector[column]([eCu, eAg, eSn, eNi]) :

sigmaCu := 5.8001·107 : sigmaAg := 1.05·sigmaCu : sigmaSn := 0.15·sigmaCu : sigmaNi := 0.2535·sigmaCu :
sigma := Vector[column]([sigmaCu, sigmaAg, sigmaSn, sigmaNi]) :
#
# Definition of Wire Radius and Plating Layer Thickness
#
a := 0.4065·10-3 : b := 0.4065·10-3 :
CT := Vector[column]([1.0·10-6, 1.0·10-6, 1.27·10-6]) :
ra := Vector[column]([b - CT[1], b - CT[2], b - CT[3]]) :
#
# Create Operational Frequency Vector
#
omega := Vector[column](99) :

N := 10 :
k := 1 :
for i from 0 to N do;
  for j from 1 to N - 1 do;
    omega[k] := 2·(evalf(Pi))·10j·j;
    k := k + 1;
  end do;
end do;

```

(cont'd next page)

```

    od;
od;
#
# Create Martrix of Skin Depths for Conductors
#
k := 'k';
k := Matrix(99, 4) :
for i from 1 to 4 do;
    for j from 1 to 99 do;
        k[j, i] :=  $\sqrt{\omega_j \mu_{j,i} \sigma_i}$ ;
    od;
od;
#
# Evaluate the Current Density in the Solid Conductors
#
Z := Matrix(99, 4) :
for i from 1 to 4 do;
    for j from 1 to 99 do;
        Z[j, i] := evalf  $\left( \frac{k[j, i] \cdot \sqrt{I}}{2 \cdot \text{Pi} \cdot \sigma_i \cdot a} \frac{\text{evalf}(\text{BesselI}(0, k[j, i] \cdot a \cdot \sqrt{I}))}{\text{evalf}(\text{BesselI}(1, k[j, i] \cdot a \cdot \sqrt{I}))} \right)$ ;
    od;
od;
#
# Plot the Impedance of the Solid Conductors
#
pRZCu := loglogplot  $\left( \frac{\omega}{\text{evalf}(2 \cdot 10^6 \cdot \text{Pi})}, \text{Re}(Z[ \dots, 1 ]), \text{gridlines} = \text{true}, \text{color} = \text{"Blue"} \right)$  :
pIZCu := loglogplot  $\left( \frac{\omega}{\text{evalf}(2 \cdot 10^6 \cdot \text{Pi})}, \text{Im}(Z[ \dots, 1 ]), \text{gridlines} = \text{true}, \text{color} = \text{"LightBlue"} \right)$  :
pRZAg := loglogplot  $\left( \frac{\omega}{\text{evalf}(2 \cdot 10^6 \cdot \text{Pi})}, \text{Re}(Z[ \dots, 2 ]), \text{gridlines} = \text{true}, \text{color} = \text{"Green"} \right)$  :
pIZAg := loglogplot  $\left( \frac{\omega}{\text{evalf}(2 \cdot 10^6 \cdot \text{Pi})}, \text{Im}(Z[ \dots, 2 ]), \text{gridlines} = \text{true}, \text{color} = \text{"LightGreen"} \right)$  :
pRZSn := loglogplot  $\left( \frac{\omega}{\text{evalf}(2 \cdot 10^6 \cdot \text{Pi})}, \text{Re}(Z[ \dots, 3 ]), \text{gridlines} = \text{true}, \text{color} = \text{"DarkViolet"} \right)$  :
pIZSn := loglogplot  $\left( \frac{\omega}{\text{evalf}(2 \cdot 10^6 \cdot \text{Pi})}, \text{Im}(Z[ \dots, 3 ]), \text{gridlines} = \text{true}, \text{color} = \text{"Violet"} \right)$  :
pRZNi := loglogplot  $\left( \frac{\omega}{\text{evalf}(2 \cdot 10^6 \cdot \text{Pi})}, \text{Re}(Z[ \dots, 4 ]), \text{gridlines} = \text{true}, \text{color} = \text{"DarkRed"} \right)$  :
pIZNi := loglogplot  $\left( \frac{\omega}{\text{evalf}(2 \cdot 10^6 \cdot \text{Pi})}, \text{Im}(Z[ \dots, 4 ]), \text{gridlines} = \text{true}, \text{color} = \text{"Red"} \right)$  :

display  $\left( \{ pRZCu, pIZCu, pRZAg, pIZAg, pRZSn, pIZSn, pRZNi, pIZNi \}, \text{labels} = \left[ \right. \right.$ 

```

(cont'd next page)

```

"Freq (MHz)", "Z (  $\frac{\text{ohms}}{\text{m}}$  )" ) :
#
# Establish Matrices for Plated Wires
#
C1Num := Matrix(91, 3) : C2aNum := Matrix(91, 3) : C2bNum := Matrix(91, 3) : CDen1
:= Matrix(91, 3) : CDen2 := Matrix(91, 3) :

C1 := Matrix(91, 3) : C2a := Matrix(91, 3) : C2b := Matrix(91, 3) : Zcoat := Matrix(91, 3) :
#
# Evaluate the Current Density in Plated Wires
#
for i from 1 to 3 do;
  for j from 1 to 91 do;
    C1Num[j, i] := -1 * ( evalf( Bessel(0, kj, i+1 * rai * sqrt(T)) ) ) * ( evalf( BesselK(1, kj, i+1 * rai
* sqrt(T)) ) ) - ( evalf( BesselK(0, kj, i+1 * rai * sqrt(T)) ) ) * ( evalf( Bessel(1, kj, i+1 * rai * sqrt(T)) ) );
    C2aNum[j, i] := (  $\frac{\sqrt{\mu_{j, i+1} \sigma_{i+1}}}{\sqrt{\mu_{j, 1} \sigma_1}}$  * ( ( -evalf( BesselK(0, kj, i+1 * rai * sqrt(T)) ) )
* ( evalf( Bessel(1, kj, 1 * rai * sqrt(T)) ) ) ) - (  $\frac{\sigma_{i+1}}{\sigma_1}$  ) * ( ( evalf( Bessel(0, kj, 1 * rai * sqrt(T)) ) )
* ( evalf( BesselK(1, kj, i+1 * rai * sqrt(T)) ) ) ) );
    C2bNum[j, i] := ( (  $\frac{\sigma_{i+1}}{\sigma_1}$  ) * ( ( -evalf( Bessel(1, kj, i+1 * rai * sqrt(T)) ) ) * ( evalf( Bessel(0, kj, 1
* rai * sqrt(T)) ) ) ) +  $\frac{\sqrt{\mu_{j, i+1} \sigma_{i+1}}}{\sqrt{\mu_{j, 1} \sigma_1}}$  * ( ( evalf( Bessel(0, kj, i+1 * rai * sqrt(T)) ) ) * ( evalf( Bessel(1, kj, 1 * rai
* sqrt(T)) ) ) ) );
    CDen1[j, i] := ( evalf( Bessel(0, kj, i+1 * b * sqrt(T)) ) ) * (  $\frac{\sqrt{\mu_{j, i+1} \sigma_{i+1}}}{\sqrt{\mu_{j, 1} \sigma_1}}$  * ( -evalf( BesselK(0,
kj, i+1 * rai * sqrt(T)) ) ) * ( evalf( Bessel(1, kj, 1 * rai * sqrt(T)) ) ) ) - (  $\frac{\sigma_{i+1}}{\sigma_1}$  ) * ( ( evalf( Bessel(0, kj, 1 * rai
* sqrt(T)) ) ) * ( evalf( BesselK(1, kj, i+1 * rai * sqrt(T)) ) ) ) );
  end for;
end for;

```

(cont'd next page)

$$CDen2[j, i] := \left( \text{evalf}(\text{BesselK}(0, k_{j, i+1} \cdot b \cdot \sqrt{T})) \right) \cdot \left( \frac{\sigma_{i+1}}{\sigma_1} \right) \cdot \left( -\text{evalf}(\text{Bessel}(1, k_{j, i+1} \cdot ra_i \cdot \sqrt{T})) \cdot \text{evalf}(\text{Bessel}(0, k_{j, i+1} \cdot ra_i \cdot \sqrt{T})) \right) + \frac{\sqrt{\mu_{j, i+1} \sigma_{i+1}}}{\sqrt{\mu_{j, 1} \sigma_1}} \cdot \left( \text{evalf}(\text{Bessel}(0, k_{j, i+1} \cdot ra_i \cdot \sqrt{T})) \cdot \text{evalf}(\text{Bessel}(1, k_{j, 1} \cdot ra_i \cdot \sqrt{T})) \right);$$

$$CI[j, i] := \frac{CINum[j, i]}{CDen1[j, i] + CDen2[j, i]};$$

$$C2a[j, i] := \frac{C2aNum[j, i]}{CDen1[j, i] + CDen2[j, i]};$$

$$C2b[j, i] := \frac{C2bNum[j, i]}{CDen1[j, i] + CDen2[j, i]};$$

$$Zcoat[j, i] := \left( k_{j, 1} \cdot \sqrt{T} \right) / \left( \left( (2 \cdot \text{evalf}(\text{Pi}) \cdot \sigma_{i+1} \cdot ra_i \cdot CI[j, i]) \cdot \text{evalf}(\text{Bessel}(1, k_{j, 1} \cdot ra_i \cdot \sqrt{T})) \right) + \frac{\sqrt{\mu_{j, i+1} \sigma_{i+1}}}{\sqrt{\mu_{j, 1} \sigma_1}} (2 \cdot \text{evalf}(\text{Pi}) \cdot \sigma_{i+1}) \cdot (C2a[j, i] \cdot (b \cdot \text{evalf}(\text{Bessel}(1, k_{j, i+1} \cdot b \cdot \sqrt{T})) - ra_i \cdot \text{evalf}(\text{Bessel}(1, k_{j, i+1} \cdot ra_i \cdot \sqrt{T}))) + C2b[j, i] \cdot (-b \cdot \text{evalf}(\text{BesselK}(1, k_{j, i+1} \cdot b \cdot \sqrt{T})) + ra_i \cdot \text{evalf}(\text{BesselK}(1, k_{j, i+1} \cdot ra_i \cdot \sqrt{T})))) \right)$$

**od;**  
**#**  
**# Plot the Impedance of the Plated Conductors**  
**#**

$$pRZcoatAg := \text{loglogplot} \left( \frac{\omega}{\text{evalf}(2 \cdot 10^6 \cdot \text{Pi})}, \text{Re}(Zcoat[ \dots, 1 ]), \text{gridlines} = \text{true}, \text{color} = \text{"Green"} \right);$$

$$pIZcoatAg := \text{loglogplot} \left( \frac{\omega}{\text{evalf}(2 \cdot 10^6 \cdot \text{Pi})}, \text{Im}(Zcoat[ \dots, 1 ]), \text{gridlines} = \text{true}, \text{color} = \text{"LightGreen"} \right);$$

$$pRZcoatSn := \text{loglogplot} \left( \frac{\omega}{\text{evalf}(2 \cdot 10^6 \cdot \text{Pi})}, \text{Re}(Zcoat[ \dots, 2 ]), \text{gridlines} = \text{true}, \text{color} = \text{"DarkViolet"} \right);$$

$$pIZcoatSn := \text{loglogplot} \left( \frac{\omega}{\text{evalf}(2 \cdot 10^6 \cdot \text{Pi})}, \text{Im}(Zcoat[ \dots, 2 ]), \text{gridlines} = \text{true}, \text{color} = \text{"Violet"} \right);$$

$$pRZcoatNi := \text{loglogplot} \left( \frac{\omega}{\text{evalf}(2 \cdot 10^6 \cdot \text{Pi})}, \text{Re}(Zcoat[ \dots, 3 ]), \text{gridlines} = \text{true}, \text{color} = \text{"DarkViolet"} \right);$$

(cont'd next page)

```

    = "DarkRed" ) :
pIZcoatNi := loglogplot(  $\frac{\omega}{\text{evalf}(2 \cdot 10^6 \cdot \text{Pi})}$ , Im(Zcoat[ .., 3]), gridlines = true, color = "Red" ) :
display( {pRZcoatAg, pIZcoatAg, pRZcoatSn, pIZcoatSn, pRZcoatNi, pIZcoatNi}, labels = [
    "Freq (MHz)", "Z (  $\frac{\text{ohms}}{m}$  )" ] ) :

```

## References

- [1] The Saturday Magazine, Volume 18, January to June, 1841, published by John William Parker, West Strand, London, ppg 142 – 144.
- [2] Veitch, H. N., “Sheffield Plate, Its History, Manufacture, and Art”, George Bell & Sons, London, 1908, ppg 64 – 71.
- [3] *Standard Specification for Tinned Soft or Annealed Copper Wire for Electrical Purposes*, American Society for Testing and Materials (ASTM) B33-10, 2010.
- [4] *Standard Specification for Silver-Coated Soft or Annealed Copper Wire*, American Society for Testing and Materials (ASTM) B298-07, 2007.
- [5] *Standard Specification for Nickel-Coated Soft or Annealed Copper Wire*, American Society for Testing and Materials (ASTM) B355-11, 2011.
- [6] *General Specification for Insulated Electrical Wire*, Mil-W-16878.
- [7] *Wire, Electrical, Fluoropolymer-Insulated, Copper or Copper Alloy*, SAE-AS22759.
- [8] *Wire, Electrical, Crosslinked Polyalkene, Crosslinked Alkane-Imide Polymer, or Polyarylene Insulated, Copper Or Copper Alloy*, SAE-AS81044.
- [9] *Detail Specification for Wire, Electric, Polyimide-Insulated, Copper or Copper Alloy*, Mil-W-81381.
- [10] Dunn, B. D. et al, “Corrosion of Silver-Plated Conductors”, *European Space Agency Journal*, Vol 8, 1984.
- [11] S. Harput. *Fields of Application of Nickel Plated Copper Conductor* [Online]. Available: [http://www.sarkuysan.com/Upload/Document/document\\_3456096f90eb4f61a619f1376fdee351.pdf](http://www.sarkuysan.com/Upload/Document/document_3456096f90eb4f61a619f1376fdee351.pdf)
- [12] T. R. Long, “Electrodeposited Memory Elements for a Nondestructive Memory”, *J. Appl. Phys.*, Supp to Vol 31, no. 5, pp. 123S -124S, May 1960.
- [13] H. K. Lotsch, “Magnetic-Field Design Considerations for a Plated-Wire memory”, *IEEE Trans. Comput.*, vol. C-18, no. 10, pp. 894-899, Oct. 1969.
- [14] J. S. Mathias and G. A. Fedde, “Plated-Wire technology: A Critical Review”, *IEEE Tran. Magn.*, vol. MAG-5, no. 4, pp. 728-751, Dec. 1969.
- [15] W. A. England, “Applications of Plated Wire to the Military and Space Environments”, *IEEE Tran. Magn.*, vol. MAG-6, no. 3, pp. 528-534, Sep. 1970.
- [16] L. D. Bolton. *Plated Wire Memory Usage on the UNIVAC Minutemen Weapon System Computer* [Online]. Available: <http://www.vipclubmn.org/Articles/PlatedWire.pdf>

- [17] R. M. Rowe, "Filter Line Wiring Designs in Aircraft," in *SAE Aerospace Technology Conference and Exposition*, Sep. 1990, pp. 1653-1658.
- [18] *EMC Cables* [Online]. Available: <http://pdf.directindustry.com/pdf/eupen-cable-division/emc-cables/20911-50776.html#search-eupen>
- [19] M. Kirschvink et al, "Interference Suppression on Motor Control Cables for Frequency Converters," in *Applied Power Electronics Conference and Exposition Annual IEEE Conference – APEC*, 1996, pp. 593-600.
- [20] *IM Products EMI Noise Suppression USB2.0 Cable LNC Series* [Online]. Available: <http://www.intermark-usa.com/products/emc/emi-absorbers/emi-noise-surpression-cable/lnc-series/>
- [21] *Wave-X Z* [Online]. Available: <http://www.arc-tech.com/cables.php>
- [22] J. C. Maxwell, *A Treatise on Electricity and Magnetism*. Oxford: Clarendon Press, 1873, vol. II, 1<sup>st</sup> ed., pp. 291-293.
- [23] J. C. Maxwell, *A Treatise on Electricity and Magnetism*. London: Henry Frowde, Oxford University Press Warehouse, Amen Corner, E.C., 1892, vol. II, 3<sup>rd</sup> ed., pp. 323-325.
- [24] O. Heaviside, "Effective Resistance and Inductance of a Round Wire," *The Electrician*, 1884, p. 583.
- [25] *Ibid.*, 1885, p. 489.
- [26] O. Heaviside, *Electrical papers*, vol.I, pp. 353, 429; vol. II, pp. 50, 97.
- [27] Lord Rayleigh, *Phil. Mag.*, 1886, pp. 382,469.
- [28] Lord Kelvin, *Journ. Soc. Tel. Eng.*, 1889, vol. 18, p. 36.
- [29] F. F. Fowle, "Electrical Properties of Compound Wires-I," *Electrical World*, vol. LVI, no. 25, pp. 1471-1475, Dec. 1910.
- [30] F. F. Fowle, "Electrical Properties of Compound Wires-II," *Electrical World*, vol. LVI, no. 26, pp. 1521-1525, Dec. 1910.
- [31] F. F. Fowle, "Electrical Properties of Compound Wires-III," *Electrical World*, vol. 57, no. 2, pp. 108-111, Jan. 1911.
- [32] A. E. Kennelly et al, "Experimental Researches on Skin Effect in Conductors," *Tran. Amer. Inst. Elec. Eng.*, vol. XXXIV, iss. 8, pp. 1379-1403, Aug. 1915, pp. 1953-2021.
- [33] H. B. Dwight, "Skin Effect in Tubular and Flat Conductors," *Tran. Amer. Inst. Elec. Eng.*, vol. XXXVII, iss. 2, pp. 1379-1403, Jul. 1918



- [34] H. B. Dwight, "Proximity Effect in Wires and Thin Tubes," *Tran. Amer. Inst. Elec. Eng.*, vol. XLII, pp. 850-859, Jan. 1923
- [35] A. H. M. Arnold, "Proximity Effect in Solid and Hollow Conductors," *Jour. IEE - Part II: Pow. Engrg.*, vol. 88, iss. 4, pp. 349-359, Aug. 1941
- [36] S. A. Schelkunoff, "The Electromagnetic Theory of Coaxial Transmission Lines and Cylindrical Shields," *Bell System Technical Journal*, vol. XIII, pp. 532-579, Oct. 1934.
- [37] N. F. Astbury, "Alternating-Current Properties of a Copper Conductor Clad in a Magnetic Sheath," *Proc. IEE*, vol. 110, no. 11, 2055-2062, Nov. 1963.
- [38] A. M. Fowler, "Radio Frequency Performance of Electroplated Finishes," *Proc. IREE Australia*, pp. 148-164, May, 1970.
- [39] T. Graf et al, "Inductance of Magnetic Plated Wires as a Function of Frequency and Plating Thickness," in *Proc. COMSOL Conf.*, Milan, 2009 [Online]. Available: <http://www.comsol.com/paper/inductance-of-magnetic-plated-wires-as-a-function-of-frequency-and-plating-thick-6921>
- [40] A. Kurs et al, "Wireless Power Transfer via Strongly Coupled Magnetic Resonances," *Science*, vol. 317, no. 5834, pp. 83-86, Jul. 2007.
- [41] NIST Digital Library of Mathematical Functions [Online]. Available: <http://dlmf.nist.gov/>
- [42] H. B. Dwight, *Tables of Integrals and Other Mathematical Data*. 4<sup>th</sup> ed. New York: The Macmillan Co., 1967
- [43] F. E. Relton, *Applied Bessel Functions*. New York: Dover Publications, 1965.
- [44] F. Bowman, *Introduction to Bessel Functions*. New York: Dover Publications, 1958.
- [45] N. W. McLachlan, *Bessel Functions for Engineers*. 2<sup>nd</sup> ed. London: Oxford University Press, Amen House, E.C.4, 1955.
- [46] L. C. Andrews, *Special Functions of Mathematics for Engineers*. 2<sup>nd</sup> ed. New York: McGraw-Hill, 1992, pp. 237-285.
- [47] M. Abramowitz and I. A. Stegun, Eds., *Handbook of Mathematical Functions (Applied Mathematics Series 55)*. Washington, DC: NBS, 1967, pp. 355-433.
- [48] D. K. Cheng, *Field and Wave Electromagnetics*. Reading, MA: Addison-Wesley, 1989.
- [49] R. W. P. King, *Fundamental Electromagnetic Theory*. New York: Dover Publications, 1963, pp. 321-356.
- [50] S. Ramo et al, *Fields and Waves in Communication Electronics*. 2<sup>nd</sup> ed. New York: John Wiley & Sons, 1984, pp. 178-183.

- [51] J. A. Stratton, *Electromagnetic Theory*. New York: McGraw-Hill, 1941, pp. 504, 524-537.
- [52] W. R. Smythe, *Static and Dynamic Electricity*. New York: McGraw-Hill, 1939, pp. 390-394.
- [53] S. Lucyszyn.(2008). *Microwave Characterization of Nickel* [Online]. Available: <http://www.piers.org/piersonline/download.php?file=MDgwMTE5MjE1NjU1fFZvbDR0bzZQYWdlNjg2dG82OTAucGRm>
- [54] R. M. Bozorth, *Ferromagnetism*. Princeton, NJ: D. Van Nostrand Co., 1951, pp. 798-803.
- [55] B. Young, "Determination of the Frequency Dependent Complex Permeability of Alloy 42," in *Proc. 44<sup>th</sup> Electronic Components and Technology Conf.*, Washington, DC, 1994, pp. 978-980.
- [56] C. T. Tsai et al, "High Frequency Inductance Measurements and Characterization of Alloy 42 and Copper Packages," in *Proc. 43<sup>rd</sup> Electronic Components and Technology Conf.*, Orlando, FL, 1993, pp. 635-640.
- [57] Y. Shlepnev and S. McMorrow, "Nickel Characterization for Interconnect Analysis," *IEEE Int. Symp. on Electromagnetic Compatibility (EMC)*, Long Beach, Ca., 2011, pp. 524-529.
- [58] J C Anderson and B Donovan, "On the Complex Permeability of Iron-Nickel Alloys at High Frequencies," *Proc. Phy. Soc., Sect. B*, vol. 70, no. 2, pp. 186-191, 1957.
- [59] G F Hodsman et al, "Magnetic Dispersion at Microwave Frequencies," *Proc. Phy. Soc., Sect. B*, vol. 62, no. 6, pp. 377-390, 1949.
- [60] A. Wieberdink, "On the Determination of the Complex Permeability of Ferromagnetic Conductors at High Frequencies," *App. Sci. Res., Sect. B*, vol.1, iss. 1, pp 439-452, 1950.
- [61] J. H. Rose et al, "Extreme Sensitivity of Eddy-Currents to the Surface Conditions of Nickel." in *Rev. Prog. Quant. Nondest. Eval.*, vol. 16, pp. 249-256, 1997.
- [62] J. H. Rose et al, "Magnetic Permeability and Eddy-Current Measurements," in *Rev. Prog. Quant. Nondest. Eval.*, vol. 14, pp. 315-322, 1995.
- [63] K. A. Kuhn.(2012). *A Simple Circuit for Measuring Complex Impedance* [Online]. Available: [http://www.kennethkuhn.com/electronics/impedance\\_measurement.pdf](http://www.kennethkuhn.com/electronics/impedance_measurement.pdf)
- [64] S. Wetterlin.(2011). *A Shunt Fixture for Low Impedance Measurements* [Online]. Available: [http://www.wetterlin.org/sam/SA/Operation/Fixture\\_LoZ.pdf](http://www.wetterlin.org/sam/SA/Operation/Fixture_LoZ.pdf)
- [65] G. F. Engen and C. A. Hoer, "'Thru-Reflect-Line': An Improved Technique for Calibrating the Dual Six-Port Automatic Network Analyzer," *IEEE Trans. Microw. Theory Tech.*, vol. MTT-27, no. 12, pp. 987-993, Dec. 1979.

- [66] J. Fleury and O. Bernard, "Designing and Characterizing TRL Fixture Calibration Standards for Device Modeling," *Appl. Microwave & Wireless*, vol. 14, no. 10, pp. 26-42, Oct. 2010.
- [67] *Agilent Network Analysis Applying the 8510 TRL Calibration for Non-Coaxial Measurements*, Agilent Technologies, Englewood, CO, Product Note 5091-3645E, 2006.
- [68] *Agilent Stripline TRL Calibration Fixtures for 10-Gigabit Interconnect Analysis*, Agilent Technologies, Englewood, CO, White Paper 5989-4897EN, 2006.
- [69] *Agilent Ultra-Low Impedance Measurements Using 2-Port Measurements*, Agilent Technologies, Englewood, CO, Application Note 5989-5935EN, 2007.
- [70] *Agilent E5070B/E5071B ENA Series RF Network Analyzers TRL/LRM Calibration*, Agilent Technologies, Englewood, CO, No. 16000-95026, 2004
- [71] C. R. Paul, *Inductance*. Hoboken, NJ: John Wiley & Sons, Inc., 2010, pg. 254
- [72] *Wideband Transformers*, North Hills Signal Processing Co. Syosset, NY, App. Note #151.
- [73] North Hills Signal Processing Co. Data Sheet. *Balun Transformers – General Purpose 1 kHz – 125 MHz* [Online]. Available: <http://www.northhills-sp.com/pdf/products-wb-general-purpose.pdf>
- [74] *Agilent Measuring Frequency Response with the Agilent E5061B LF-RF Network Analyzer TRL/LRM Calibration*, Agilent Technologies, Englewood, CO, Application Note 5990-5578EN, 2010
- [75] I. Novak et al. *Accuracy Improvements of PDN Impedance Measurements in the Low to Middle Frequency Range* [Online]. Available: [http://electrical-integrity.com/Paper\\_download\\_files/DC10\\_12-TH3\\_Novak-Mori-Resso.pdf](http://electrical-integrity.com/Paper_download_files/DC10_12-TH3_Novak-Mori-Resso.pdf)
- [76] SCSI PIP Committee. *Cable Attenuation Testing* [Online]. Available: <http://ftp.t10.org/ftp/t10/document.00/00-386r0.pdf>
- [77] E. J. Tuohy et al, "Transient Resistance of Conductors," *IEEE Trans. Power App. Syst.*, vol. PAS-87, no. 2, pp. 455-462, Feb. 1968.
- [78] K. W. Miller, "Diffusion of Electric Current into Rods, Tubes, and Flat Surfaces," *AIEE Trans.*, vol. 66, pp. 1496-1502, 1947.
- [79] A. Grumet, "Penetration of Transient Electromagnetic Fields into a Conductor," *Jour. App. Phys.*, vol. 30, no. 5, pp. 682-686, May 1959.
- [80] P. Silvester, "Modal Network Theory of Skin Effect in Flat Conductors," *Proc. IEEE*, vol. 54, no. 9, pp. 1147-1151, Sep. 1966.

[81] L. M. Vallese, "Diffusion of Pulsed Currents in Conductors," *Jour. App. Phys.*, vol. 25, no. 2, pp. 225-228, Feb. 1954.

## Biographical Information

Bob Scully is an IEEE Fellow, a registered Texas Professional Engineer, and holds an International Association for Radio, Telecommunications and Electromagnetics (iNARTE) Certification as an EMC Engineer and an iNARTE Certification as a Senior EMC Design Engineer, as well as having completed an EMC Certification Program with the University of Missouri Rolla.

Bob has over 20 years of experience in military and commercial aviation electrical and electronics engineering, and specializes in electromagnetics compatibility (EMC). Since June of 2000, Bob Scully has been serving as the Johnson Space Center Electromagnetics Environmental Effects (E3) Group Lead Engineer. Bob leads a mixed staff of contractors and civil servants, and is responsible for the electromagnetic interference (EMI) control laboratory facility. The E3 Group supports local project design and development activities for the Space Station Program, and for new developmental programs such as the Multi-Purpose Crewed Vehicle (MPCV). Bob also supports other duties as assigned by the Agency, including special assignments from the NASA Engineering Safety Council (NESC). Bob served as Senior Co-Chair of the Space Shuttle E3 Control Technical Panel for 10 years, until retirement of the Shuttle Program in 2011.

Within the Institute of Electrical and Electronics Engineers (IEEE) EMC Society, Bob has served as Chair of Technical Committee 1 (EMC Management), Technical Committee 4 (EMI Control), and the Technical Advisory Committee (TAC). Bob served as the Vice President of Technical Services for a number of years, and was recently elected as the President of the IEEE EMC Society. Bob and his wife Elizabeth married in 1974, and have two children and six grandchildren.